Dalton Transactions

ROYAL SOCIETY OF CHEMISTRY

PERSPECTIVE

View Article Online
View Journal | View Issue

Cite this: *Dalton Trans.*, 2026, **55**, 40

Fluorophores to fighters: BODIPY-metal complexes as next-gen anticancer prodrugs

Twara Kikani, Krutika Patel and Sonal Thakore *

Metal-coordinated complexes have been employed as effective anti-cancer agents with *cis*-platin being the foundation for the development of metal-based therapeutics. However, their use is greatly limited by their systemic toxicity, drug resistance and non-targeted approach. Progressing drug resistance has led to the use of combinatorial approaches for a multifaceted attack on cancer. Photodynamic therapy (PDT) is a clinically approved adjuvant chemotherapy that involves the use of a photosensitizer (PS), light and endogenous molecular oxygen ($^3O_2$). Boron-dipyrromethene (BODIPY) dyes are a class of fluorophores that serve as promising PSs with excellent light-activated reactive oxygen species (ROS) generating capacity (for PDT) and light-to-heat conversion (for PTT) causing the thermal ablation of cancer cells. Conjugating a metal-based drug along with a PS and a targeting ligand to design a prodrug acts as a "magic packet" to target various cancers. This review elaborates the advances in the development of metallo-prodrugs adorned with a BODIPY cage as cancer theranostics. It highlights the engineering marvel of constructing prodrugs with high specificity and organelle-targeting ability.

Received 16th July 2025,
Accepted 29th September 2025

DOI: 10.1039/d5dt01667c

rsc.li/dalton

1. Introduction

Despite substantial progress in biomedical research and healthcare interventions, cancer remains one of the leading causes of mortality worldwide, with the global fatality rate approaching an alarming level of 8 million deaths a year.[1] Conventional treatment modalities including chemotherapy, radiotherapy, and surgical resection often face limitations due to their high mutagenicity, rapid proliferation, and metastasis of neoplastic cells, which contribute to therapeutic resistance and disease recurrence.[2] In response to these challenges, recent advances in cancer therapy have focused on novel and

Department of Chemistry, Faculty of Science, The Maharaja Sayajirao University of Baroda, Vadodara 390 002, India. E-mail: chemistry2797@yahoo.com, sonal.thakore-chem@msubaroda.ac.in

Twara Kikani

Ms Twara Kikani is presently pursuing her PhD degree at the Department of Chemistry, Faculty of Science, The Maharaja Sayajirao University of Baroda, Vadodara, India, under the guidance of Prof. Sonal Thakore. She is currently working as a Senior Research Fellow, developing photoluminescent nanoplatforms for cancer therapy. She received her BSc degree in Chemistry and MSc degree in Organic Chemistry from The Maharaja Sayajirao University of Baroda. Her research interest includes stimuli-responsive polymer systems for controlled drug release. She has 8 publications in Scopus-indexed journals to her credit.

Krutika Patel

Ms Krutika Patel is presently pursuing her PhD degree at the Department of Chemistry, Faculty of Science, The Maharaja Sayajirao University of Baroda, Vadodara, India, under the guidance of Prof. Sonal Thakore. She is currently working as a Junior Research Fellow. She received her BSc degree in Chemistry and MSc degree in Organic Chemistry from The Maharaja Sayajirao University of Baroda. Her research interest includes polymeric carrier systems for biological applications. She has 2 publications in Scopus-indexed journals to her credit.

targeted approaches such as immunotherapy,[3] photodynamic therapy (PDT),[4] photothermal therapy (PTT),[5] sonodynamic therapy,[6] and ferroptosis-based interventions.[7] These emerging strategies are being actively investigated as both monotherapies and combinatorial therapies with existing treatment regimens, aiming to improve specificity, reduce systemic toxicity, and overcome resistance mechanisms associated with traditional therapies.

Surgery combined with chemotherapy is typically employed as the first-line treatment for many solid tumors.[8] However, this approach often proves ineffective in advanced or metastatic stages, where cancer spreads beyond the primary site and systemic control becomes critical. Repetitive drug administration induces multi-drug resistance (MDR) in cancer cells, and the demerits of ionizing radiation are countless.[9,10]

This directed extensive research towards photodynamic therapy (PDT) as an adjuvant therapy for cancer management. It involves the systemic delivery of photosensitizers (PSs), which preferentially accumulate at the tumor site through passive targeting mechanisms.[11] This selective accumulation is largely attributed to the distinct microenvironmental characteristics of tumor tissues such as leaky vasculature and poor lymphatic drainage compared with normal tissues.[12] In addition to a photosensitiser (PS), PDT typically employs light and endogenous molecular oxygen ($^3O_2$). Together, these components synergistically induce rapid generation of reactive oxygen species (ROS), ultimately leading to cancer cell death.[13] It is a non-invasive technique and can be administered in repeated doses.

Boron dipyrromethene (BODIPY) derivatives are a class of organoboranes that are excellent photosensitizers.[14–16] They exhibit high sensitivity, unique high fluorescence quantum yields, and a large molar extinction coefficient, and they are characterized by high stability. Their strong fluorescence not only enhances their potential as effective photosensitizing agents but also enables simultaneous bioimaging capabilities.[17,18] Furthermore, its ability to coordinate with metal ions enables the design of metalated BODIPY-conjugated prodrugs, in which a metal-based therapeutic agent is encased within the BODIPY photosensitizer framework.[19]

A prodrug is an inactive or less active form of a drug that becomes pharmacologically active only after it is metabolized or chemically transformed inside the body.[20] This transformation is typically carried out by enzymes, pH changes or other physiological conditions.[21–23] This approach aids in minimizing the toxic effects of the parent drug with enhanced pharmacological effects. There are various reports wherein the scientists have designed BODIPY-based prodrugs with common organic chemotherapeutic agents such as camptothecin[24] and tirapazamine.[25] However, due to the well-documented adverse effects associated with such alkylating agents, designing prodrugs based on metalated chemotherapeutics presents a more strategic alternative enabling the integration of the parent metallodrug with a photosensitizer such as BODIPY and a tumor-targeting moiety for enhanced specificity and therapeutic control.

Pondering over the above discussion, this review encapsulates the recent design strategies of BODIPY-caged metallodrugs decorated with targeting ligands. This review highlights the recent advancements in revitalizing metal-based drugs, which were once at the forefront of anti-neoplastic research but have since been overshadowed by the widespread clinical adoption of organic chemotherapeutics such as doxorubicin and paclitaxel (Scheme 1).

Sonal Thakore

Dr Sonal Thakore is a Professor and a leading Researcher in the Department of Chemistry, Faculty of Science, The Maharaja Sayajirao University of Baroda, Vadodara, India. She received her MSc in Organic Chemistry and PhD in Chemistry from the Maharaja Sayajirao University, Vadodara. She has teaching and research experience of over 25 years. Her research interests are synthesis and applications of functionalised nanomaterials for drug delivery, catalysis and environmental remediation. She has published over 90 research papers in international journals. She has authored two books and 5 book chapters and has also been granted 4 Indian Patents. She has delivered talks and presented papers in several international and national conferences. She has supervised 10 PhD students to completion and is currently mentoring 8 other doctoral scholars.

2. Organic alkylating agents *vs.* metal-based anti-cancer drugs

Organic anti-cancer drugs primarily act through DNA alkylation, a mechanism that is known to promote the development of multidrug resistance (MDR) and increase mutagenicity in cancer cells over time. These challenges can be effectively addressed by switching to metal-based anti-cancer agents, such as cisplatin, which offer alternative mechanisms of action such as DNA cross-linking *via* coordination and redox

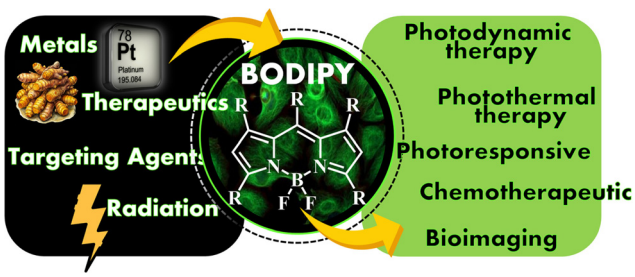

Scheme 1 Schematic combining the key themes of this review.

Table 1 Advantages of metal-based drugs over alkylating agents

Feature	Organic alkylating drugs	Metallodrugs	Ref.
Mechanism variety	Alkylation (limited)	Variety (DNA crosslinking, ROS generation)	27 and 28
Selectivity	Poor	Tunable to be selective	29 and 30
MDR	Common	Harder to develop	31 and 32
Customization	Difficult	Easy *via* co-ordination chemistry	33
Delivery	Less controlled (required specially carriers, not easy to design prodrugs)	Can be engineered to be target specific with easy prodrug strategy	34 and 35
Multi-functionality	Rare	Common (PDT, redox, enzyme response)	36

activity with improved therapeutic profiles.[26] A concise comparison between organic alkylating agents and the metallodrugs is enlisted in Table 1.

Cisplatin, a platinum (Pt) coordination complex, was first synthesized by Italian scientist Michel Peyrone in the 19th century, which was initially known as Peyrone's chloride. Its anti-cancer properties were later discovered accidentally by Barnett Rosenberg at Michigan State University in 1965, during a series of experiments investigating the effects of electric fields on bacterial growth.[37] It later got approved by the US FDA in 1975 for use in testicular and ovarian cancers. However, cisplatin soon suffered a downfall owing to its nephrotoxicity, lack of specificity, efficiency limited to certain cancers and poor pharmacokinetics.[38] This caused a major shift in research towards other metallodrugs such as ruthenium (Ru),[39] copper (Cu)[40,41] and cobalt (Co).[42] Nevertheless, the use of simple metal complexes alone struggled to keep pace with the evolving complexity and therapeutic demands of emerging cancer types.

This paved the way for the development of metalloprodrugs with stimuli-responsive behaviour and target specificity, retaining their therapeutic efficacy while minimizing off-target toxicity to healthy cells often enhanced by complementary technologies such as PDT and PTT.

3. Photophysics of BODIPY and its metal conjugates and their role in PDT and PTT

BODIPY dyes represent promising photosensitizers (PSs) for cancer therapy modalities such as photodynamic therapy (PDT) and photothermal therapy (PTT), owing to their high molar extinction coefficients, strong intrinsic fluorescence, and robust photostability. The underlying photophysics of a PS proceeds along the following general sequence:[43]

• Upon absorption of a photon, the PS is promoted to its first excited singlet state (S_1). From S_1, it may decay by fluorescence, undergo non-radiative relaxation, or undergo intersystem crossing (ISC) to access the triplet excited state (T_1).

• Once in the triplet state, the PS can produce reactive oxygen species (ROS) by different mechanistic pathways, the two principal pathways being type I and type II.

In the type I mechanism, the photosensitizer in its triplet excited state (T_1) engages in electron transfer or hydrogen atom abstraction reactions with biomolecular substrates. These processes generate radical or radical-ion intermediates (for example, the PS becoming a radical anion and the substrate a radical cation). In the presence of molecular oxygen, these radical species can further react to form ROS such as superoxide ($O_2^{\bullet-}$), hydrogen peroxide (H_2O_2), and hydroxyl radicals ($^{\bullet}OH$). Type I pathways are generally more effective under hypoxic (low-oxygen) conditions. In contrast, type II processes require sufficient oxygen: the PS in T_1 transfers energy directly to ground-state molecular oxygen ($^3O_2$), producing singlet oxygen ($^1O_2$). Because $^1O_2$ generation depends on oxygen availability, type II PDT is significantly less effective in hypoxic environments.[44]

BODIPY can be tailored to follow a desired pathway as the dominant pathway. Metal conjugation can influence various photophysical properties of a BODIPY-based photosensitizer, thereby improving its ability to generate reactive oxygen species (ROS) *via* both type I (electron or H–atom transfer) and type II (energy transfer to $O_2 \rightarrow {}^1O_2$) pathways. The incorporation of heavy-atom substituents enhances spin–orbit coupling, thereby increasing the rate of intersystem crossing (ISC) from the excited singlet state to the triplet manifold. This leads to higher triplet state populations and longer triplet lifetimes, which favour reactive oxygen species (ROS) generation especially *via* type II energy transfer to molecular oxygen.[45]

4. Targeting cellular organelles with metal–BODIPY conjugates

Organelle-targeted therapies are an emerging frontier in cancer treatment, aiming to enhance the precision and efficacy of anti-cancer agents by directing them to specific subcellular compartments. Organelle-targeted therapies majorly include the nucleus, mitochondria, endoplasmic reticulum (ER) and Golgi apparatus.[46]

Cisplatin, a prototypical platinum-based chemotherapeutic agent, exhibits its antiproliferative effects primarily through nuclear DNA targeting. Upon entering the cell, it undergoes aquation, replacing its chloride ligands with water molecules, which enhances its electrophilic reactivity. This activated form binds with purine bases of the DNA, predominantly guanine, forming intra-strand and interstrand cross-links. These adducts induce significant structural distortions in the DNA helix, hindering essential processes such as replication and transcription. The resulting DNA damage activates cellular repair mechanisms, notably the nucleotide excision repair

(NER) pathway.[47] However, this very NER can contribute to resistance in certain cancers against some common drugs by repairing the drug-induced DNA damage, potentially reducing treatment effectiveness. Therefore, strategies that circumvent this pathway offer a promising approach to enhance the efficacy of DNA-damaging agents, particularly in tumors exhibiting high NER activity.

Mitochondrial localization is a strategic approach in cancer therapy, particularly when aiming to negate this effect. By targeting therapeutic agents directly to the mitochondria, this strategy exploits the absence of NER machinery in the mitochondria, thereby enhancing the efficacy of treatments that induce DNA damage within this organelle.

5. Development of BODIPY-decorated metalloprodrugs

5.1. BODIPY-adorned cisplatin prodrugs

Cisplatin is one of the most effective and widely used platinum-based anticancer agents, primarily used to treat various cancers, including testicular, ovarian, bladder, and lung cancers.[48] Its mechanism of action involves forming covalent bonds with DNA, leading to intrastrand and interstrand cross-links that disrupt DNA replication and transcription, thereby inducing cell cycle arrest and apoptosis.[49] Despite its efficacy, cisplatin is associated with several dose-limiting side effects, including nephrotoxicity, neurotoxicity, ototoxicity, myelosuppression, and gastrointestinal disturbances. Resistance to cisplatin remains a significant challenge in clinical oncology. Mechanisms of resistance include reduced drug uptake, increased efflux, enhanced DNA repair, and alterations in apoptotic signalling pathways. To overcome these limitations, cisplatin is often used in combination with other chemotherapeutic agents or in nanoparticle formulations to enhance its efficacy and reduce toxicity. Research studies across the globe have taken varied approaches to counteract these limitations.

Initial attempts were made to design Pt(IV)-based octahedral prodrugs using oxidized cisplatin or its analogues, as they were less reactive than the classical Pt(II) drugs, thereby negating the toxic effects of cisplatin. Despite significant advancements in developing efficient anticancer Pt(IV) prodrugs, these complexes still exhibit limited selectivity and are susceptible to nonspecific interactions in the bloodstream. This lack of selectivity can lead to unintended side reactions, reducing their therapeutic efficacy and increasing the risk of adverse effects. In response to this, Spector *et al.* have designed a cisplatin-derived Pt(IV) prodrug capable of the photoinduced release of the cytotoxic agent.[50] Two BODIPY-based blue light active complexes [Pt-1 (**1**) and Pt-2 (**2**)] were synthesized using carbamate and triazole linkers, respectively. Cytotoxicity studies revealed that both Pt(IV) prodrugs exhibited no toxicity in the dark but became cytotoxic to MCF-7 cells upon low-dose blue light irradiation, with the observed effect attributed solely to the release of cisplatin from the Pt(IV) complexes. Further, density functional theory (DFT) modelling and ΔG° PET (Photoinduced Electron Transfer) estimation were carried out to reveal the action mechanism of these complexes. These calculations indicate that the key step in the light-induced release of cisplatin from Pt(IV) prodrugs involves photoinduced electron transfer from the singlet excited state of the BODIPY axial ligand to the Pt(IV) centre. This process leads to the formation of an anion-radical intermediate, facilitating the reduction of Pt(IV) to Pt(II) and subsequent cisplatin release upon photoexcitation.

Similarly, Yao *et al.* have designed green-light-active self-reducing carboplatin-based Pt(IV) prodrug functionalized with BODIPY as a photoabsorber (BODI–Pt) (**3**) at the axial position, as shown in Fig. 1a.[51] It was found to be 39 times more effective than native carboplatin against human breast cancer cell lines (MCF-7). BODI–Pt induces programmed cell death by binding to genomic DNA, causing disruption of DNA replication and transcription, leading to cell cycle arrest, particularly at the G2/M phase, and activates apoptotic pathways. Additionally, it generates ROS upon irradiation, which further contribute to cytotoxicity by inducing mitochondrial dysfunction and oxidative stress.

The actual drug form of platinum-based chemotherapeutic agents is Pt(II). However, owing to the toxicity of this form, prodrugs are usually designed as platinum(IV), which is reduced *in situ* to Pt(II) in a controlled fashion. Pt(IV) complexes being octahedral are kinetically more stable, and hence, much more resistant to premature activation. Positioning the ligands axially has a positive influence on stability and controlled activation. To study the implication of this, Yao *et al.* synthesized a series of ten carboplatin prodrug derivatives (**4**) (Fig. 1b), typically to study the influence of placing the BODIPY axially opposite to the ligands on the photoactivation of Pt(IV).[52] The researchers designed two series of prodrugs: **OH$_n$C** (containing a hydroxido ligand at the opposite axial position) and **AC$_n$C** (containing an acetato ligand), where '*n*' indicates the number of CH_2 groups (n = 2 to 8) in the linker between the BODIPY core and the platinum(IV) centre. They investigated how the distance between the photoabsorber and the platinum centre (linker length) and the nature of the opposite axial ligand (hydroxido *vs.* acetato) influence the photoactivation rate. The prodrug series demonstrated at least two times higher platinum accumulation in human ovarian carcinoma cells (A2780) than carboplatin alone. While OH$_n$C exhibited greater accumulation than AC$_n$C, acetato complexes were photoactivated much quicker than OH$_n$C. AC$_3$C was photoactivated the quickest among the acetylated prodrugs with an IC_{50} value of 43.8 μM under irradiation. The findings suggest that optimizing axial ligands, particularly by incorporating an acetato ligand and a linker of appropriate length (*e.g.* AC$_3$C), can promote efficient photoactivation and may contribute to the future rational design of photoactivable carboplatin-based anticancer prodrugs.

Krasnovskaya and group have developed dual-action nanoformulation photothermal imaging (PTI), combined with photodynamic therapy (PDT) and photothermal therapy (PTT).[53] Being inspired from the fascinating properties of BODIPY-based J-aggregates, they have fabricated a cisplatin-

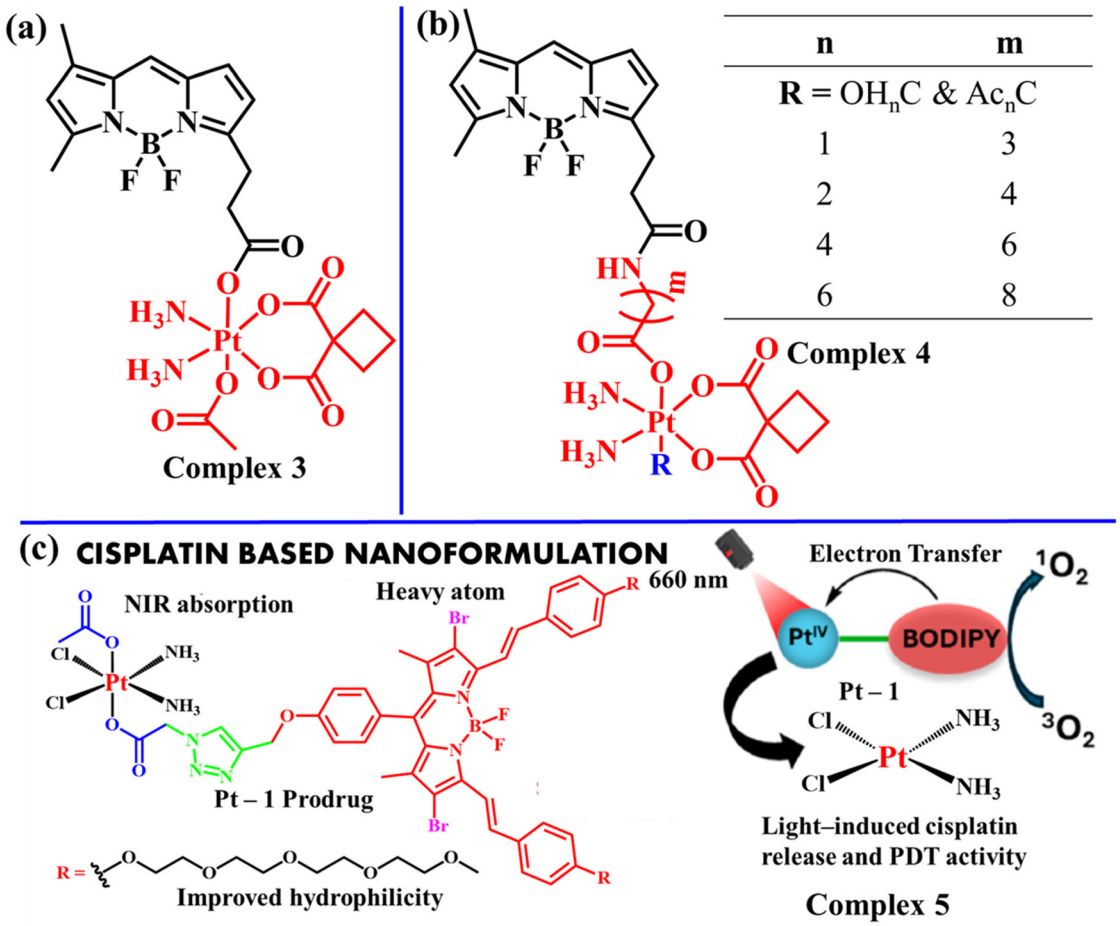

Fig. 1 Structures of platinum-based (a) complex **3** [51] [adapted from ref. 51 with permission from the American Chemical Society, copyright 2020] and (b) complex **4** [52] [adapted from ref. 52 with permission from the Royal Society of Chemistry copyright 2021]. (c) Cisplatin-based nanoformulation and its mechanism of dual action under 660 nm irradiation[53] [adapted from ref. 53 with permission from the American Chemical Society, copyright 2024].

derived prodrug adorned with a tetraethylene glycol (TEG)-bearing BODIPY unit (**5**) (Fig. 1c). Owing to its capability to self-aggregate, it shows promising results for *in vivo* tumor fluorescent imaging. This nanoprodrug has enhanced water solubility due to the TEG unit and consequently better bioavailability. Increased water availability also results in enhanced PTT activity, long bloodstream circulation time, and the ability to accumulate in the tumor. It showed promising anti-tumor behaviour when assessed in a murine colorectal carcinoma (CT-26) *in vivo* model.

Sun *et al.* initiated the designing of a simple cisplatin-based prodrug with BODIPY-labelled platinum with one of the chloride ions being replaced by the pyridine group of BODIPY. The fluorescent BODIPY–Pt conjugate (**6**) demonstrated mitochondrial targeted potent inhibition of cellular proliferation in human cervical carcinoma (HeLa) and human breast cancer (MCF-7) cell lines, with half maximal inhibitory concentrations (IC_{50}) of 27.37 μM and 12.14 μM, respectively.[54]

Multiple variants of BODIPY-appended platin-based formulations were then developed by researchers. Raza *et al.* have developed a mitochondria-targeted BODIPY-conjugated imidazoplatin derivative (**7**) for cellular imaging (Fig. 2a).[19] In addition to mitochondrial localization, it demonstrated minor endoplasmic reticulum (ER) localization. This aids in enhanced cellular apoptosis, thereby exhibiting an extremely low IC_{50} value.

As an advancement to the previous work, Raza *et al.* developed a BODIPY-appended pyriplatin-B complex for lung and breast cancers, as illustrated in Fig. 2b.[55] The anticancer studies were carried out on A549 (human lung carcinoma) and MCF-7 (human breast adenocarcinoma). Pyriplatin-B was found to be more potent than imidazoplatin as a chemotherapeutic drug, as it impedes the RNA II polymerase activity. They typically prepared three complexes (complex **8**, **9** and **10**) with three different BODIPY ligands (L^1 = non-iodinated, L^2 = monoiodinated and L^3 = diiodinated), respectively. The quantum yield for each of the complexes followed the order of **8** > **9** > **10**. Thus, complex **9** with the highest fluorescence was a good cellular imaging candidate, while the non-fluorescent complex **10** is a potential PDT agent. Surprisingly, the properties of complex **9** falls somewhere between these two, and thus, possess the characteristics of both

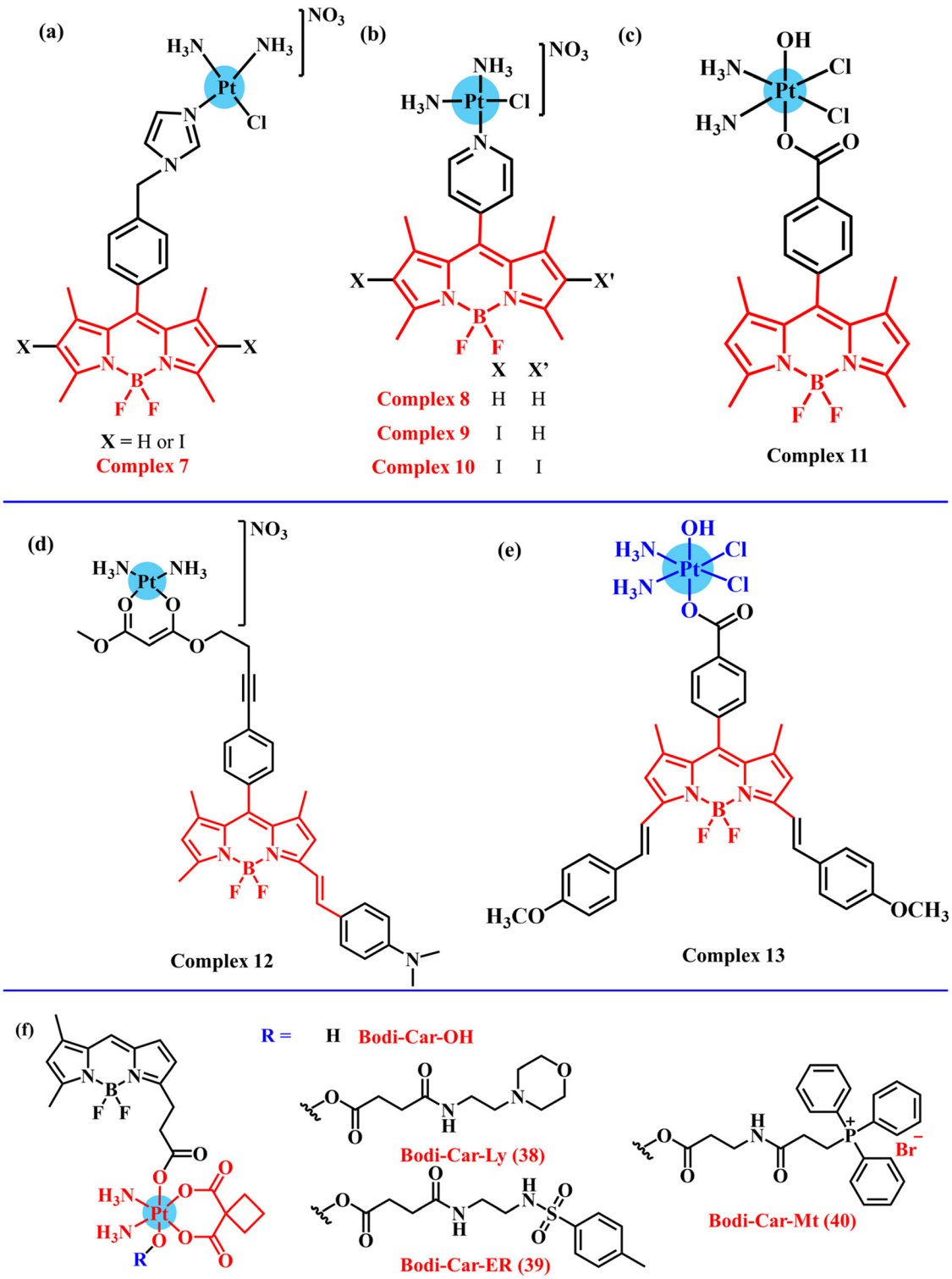

Fig. 2 Structures of platinum-based (a) complex **7**[19] [adapted from ref. 19 with permission from the American Chemical Society, copyright 2017], (b) complexes **8–10**[55] [adapted from ref. 55 with permission from the American Chemical Society, copyright 2018], (c) complex **11**[56] [adapted from ref. 56 with permission from Elsevier, copyright 2021], (d) complex **12**[57] [adapted from ref. 57 with permission from the American Chemical Society, copyright 2021], (e) complex **13**[58] [adapted from ref. 58 with permission from the Royal Society of Chemistry, copyright 2022] and (f) complexes **14–16**[59] [adapted from ref. 59 with permission from the Royal Society of Chemistry, copyright 2025].

these complexes making it suitable for bioimaging as well as photodynamic therapy.

Bera *et al.* have developed a new cisplatin-derived chemotherapeutic and a PDT prodrug named Oxoplatin-B (Fig. 2c).[56] This platinum(IV) complex ($[Pt(NH_3)_2Cl_2(\mathbf{L_1})(OH)]$) (**11**) of 4-methylbenzoic acid ($H\mathbf{L_1}$) functionalized with 4,4-difluoro-4-bora-3a,4a-diaza-s-indacene) appended with BODIPY exhibited an excellent Pearson's correlation coefficient (PCC) value of 0.96. PCC is a parameter that quantifies the extent of localization of a fluorescent molecule inside a cell. It demonstrated remarkable green light-activated phototherapeutic activity in various cancer cells [Human breast cancer (MCF-7), cervical cancer (HeLa) and lung cancer (A549) cells] with half minimal inhibitory concentration (IC_{50}) ranging from 1.1 to 3.8 μM.

Ramu *et al.* designed another prodrug meloplatin-B, which is a Pt(II) complex $[[Pt(A\text{-}BOD)(NH_3)_2](NO_3)$ (**12**) or (Pt-A-BOD)] consisting of a monoanionic O,O-donor methyl malonyl moiety conjugated to a monostyryl BODIPY ligand (HA-BOD) (Fig. 2d).[57] It is an efficient near-IR-light-active photodynamic therapy (PDT) agent exhibiting rapid cellular uptake in lung cancer A549 cells through an energy-dependent pathway. The complex induced a marked disruption of mitochondrial membrane potential, triggering the mitochondrial-mediated apoptosis *via* a singlet oxygen pathway in A549 lung adenocarcinoma cells. Further, the compound demonstrated superior photostability and reduced photobleaching, rendering it a promising theranostic agent for dual-modal applications: near-infrared fluorescence imaging and PDT. The same group of scientists have designed a Pt(IV) prodrug $[Pt(NH_3)_2Cl_2(OH)(L_1)]$ (**13**), having an axial carboxylate ligand HL_1 with a covalently linked red-light-active BODIPY moiety (Fig. 2e).[58] The prodrug demonstrated rapid activation upon red light irradiation under a reducing environment, which is a characteristic of tumor microenvironment while it remained largely stable in the dark. The non-toxic Pt(IV) prodrug efficiently generated singlet oxygen through a type II energy transfer mechanism, yielding reactive oxygen species (ROS) in high quantum yields. The anti-cancer efficiency of the complex was assessed against HeLa and MCF-7 cancer cell lines, where it showed sub-micromolar IC_{50} values on red light irradiation which are 100-fold greater than that of the clinically approved cisplatin as well as their previously developed green-light-activated analogue (**12**). This red emissive complex exhibited localization in the endoplasmic reticulum (ER) in addition to the mitochondria.

Xu *et al.* attempted to design a bunch of platinum derivatives targeted towards the lysozyme (Ly), mitochondria (Mt) and endoplasmic reticulum (ER).[59] Initially, they synthesized three oxaplatin-based prodrugs, namely, Bodi–Oxa–Ly, Bodi–Oxa–ER, and Bodi–Oxa–Mt. Despite being identified as potential candidates, the BODIPY–Oxa–Pt(IV) prodrugs demonstrated relatively low phototoxicity across various cancer cell lines. When evaluated for phototoxicity against human ovarian cancer (A2780), lung cancer (A549), and cisplatin-resistant A549 (A549cisR) cell lines, the phototoxicity index (PI) that is defined as the ratio of the IC_{50} value in the dark to the IC_{50} value under irradiation was found to be less than 3 for all cell lines. Furthermore, these prodrugs did not exhibit enhanced phototoxicity compared to oxaliplatin. Specifically, the phototoxicity fold increase (FI), calculated as the ratio of the IC_{50} value for oxaliplatin under irradiation to the IC_{50} value for BODIPY–Oxa–Pt(IV) prodrugs under irradiation, was less than 1 for all cell lines. To circumnavigate this drawback, they synthesized similar derivatives with carboplatin referred to as Bodi–Car–Ly (**14**), Bodi–Car–ER (**15**), and Bodi–Car–Mt (**16**). All three complexes were decorated with different organelle-specific ligands (Fig. 2f). Derivative **14** adorned morpholine, while derivatives **15** and **16** were appended with phenyl sulfonamide and (2-carboxyethyl)triphenylphosphonium bromide, respectively, in addition to BODIPY. This study was further extended to A2780cisR, HeLa, HepG2 and HFF. Among the 3 complexes, the mitochondria targeting complex (**16**) showed the best results and among all the cell lines under consideration, it showed the highest photocytotoxicity against HeLa cells. This infers that mitochondrial targeting leads to the highest anti-cancer property and enhances the efficacy by exploiting their pivotal role in energy production and apoptosis regulation.

5.1.1. Sugar-modified cisplatin-derived prodrugs. Lately, researchers have been working on sugar-based BODIPY-appended cisplatin derivatives. Torre and group have reported a glycosylated BODIPY-incorporated Pt(II) metallacyclic prodrug (**17**) (Fig. 3a).[60] This specific strategy was very smartly employed to target GLUT1, which is one of the most over-expressed in a tumor microenvironment out of the human glucose transporters (GLUTs) reported so far.[61] Therefore, glucose was conjugated with the triangular skeleton of the BODIPY–Pt(II) prodrug with the aim to promote cellular uptake *via* the Warburg effect.[62] The synergistic efficacy of the cyclic prodrug was assessed for HT29, HEK239 and A549 cell lines for its dual action of chemo- and photodynamic-therapy. Another glucose-appended BODIPY–Pt prodrug (**18**) was constructed by Chakravarty and group, which was designed to activate under near-infrared (NIR) light irradiation to work against HeLa, MCF-7 and A549 cell lines (Fig. 3b).[63] The prodrug resulted in an IC_{50} value in the range of 2.3–24.7 μM under NIR irradiation, and interestingly, it demonstrated mitochondrial targeting ability.

5.2. Non-platinated BODIPY metalloprodrugs

Despite being a cornerstone of cancer treatment, platinum-based chemotherapy faces significant challenges due to the development of acquired drug resistance. Beyond platinum-based agents, emerging metallodrugs incorporating elements such as ruthenium, cobalt and copper are gaining attention in cancer photodynamic therapy, owing to their ability to generate reactive oxygen species under light activation, adaptable chemical structures, and potential to overcome limitations associated with traditional chemotherapeutics.

Angela Casini and team have developed three novel Pd_2L_4 metallacages $C1{\cdot}BF_4$ (**19**), $C1{\cdot}NO_3$ (**20**), and $C2{\cdot}NO_3$ (**21**) by the self-assembly of two types of bispyridyl ligands featuring 3,5-bis(3-ethynylpyridine)phenyl cores, *exo*-functionalized with a fluorescent BODIPY moiety. As observed in Fig. 4a, these cages

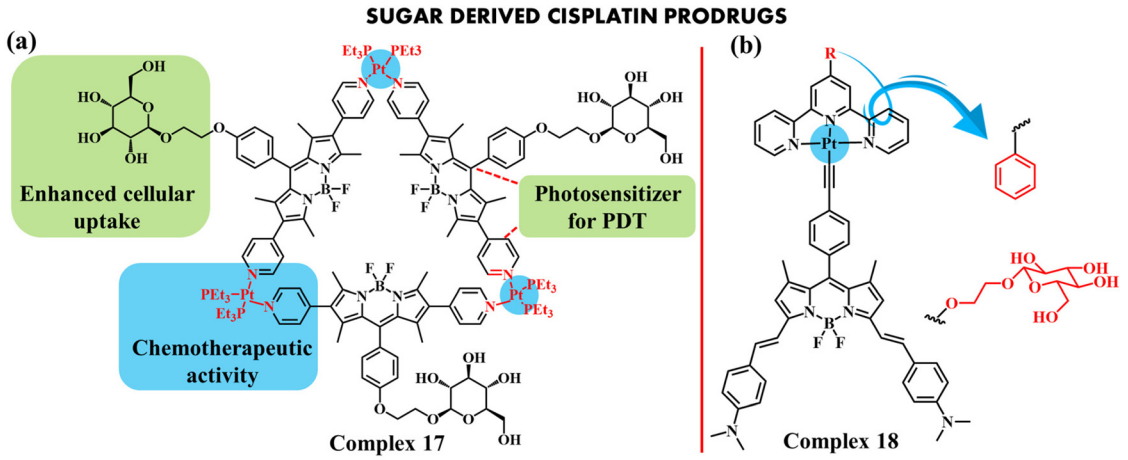

Fig. 3 Sugar-based BODIPY-adorned cisplatin prodrug (a) complex **17** [60] [adapted from ref. 60 with permission from the American Chemical Society, copyright 2023] and (b) complex **18** [63] [adapted from ref. 63 with permission from the American Chemical Society, copyright 2018].

incorporate Pd(II) ions and have been utilized in imaging applications.[64] The stability of the cages C1·BF_4, C1·NO_3, and C2·NO_3 in an aqueous solution was evaluated by UV-visible spectroscopy. Their interactions with physiologically relevant glutathione (GSH) concentrations were investigated by NMR spectroscopy, which revealed partial disassembly of the cages in the presence of GSH. These metallacages exhibit excellent luminescent properties, with quantum yields ranging from 50% to 70% and they show excitation in the visible region. Furthermore, the cages efficiently encapsulate the anticancer

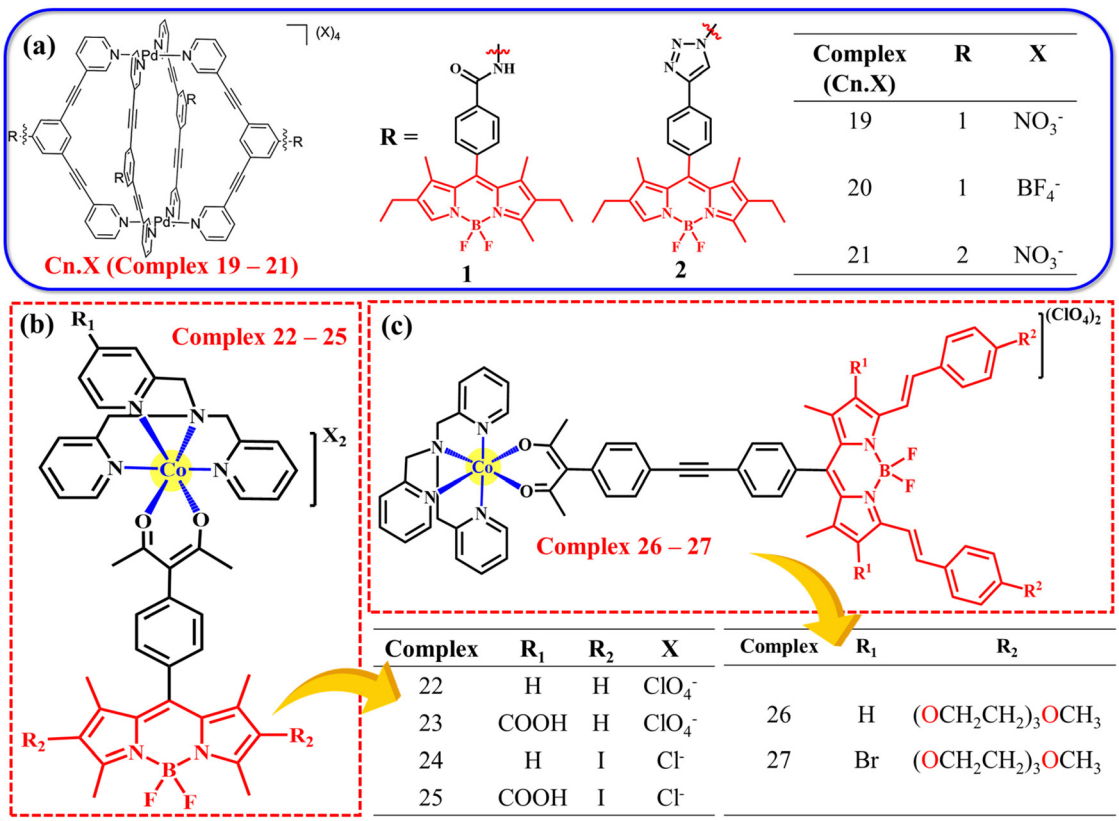

Complex (Cn.X)	R	X
19	1	NO_3^-
20	1	BF_4^-
21	2	NO_3^-

Complex	R_1	R_2	X
22	H	H	ClO_4^-
23	COOH	H	ClO_4^-
24	H	I	Cl^-
25	COOH	I	Cl^-

Complex	R_1	R_2
26	H	$(OCH_2CH_2)_3OCH_3$
27	Br	$(OCH_2CH_2)_3OCH_3$

Fig. 4 (a) Structure of Pd_2L_4 metallacages (complex **8–10**) with *exo*-functionalised BODIPY fluorophores[64] [adapted from ref. 64 with permission from Elsevier, copyright 2019]. Chemical structures of Co(III)-based (b) complexes **22–25** [65] [adapted from ref. 65 with permission from the American Chemical Society, copyright 2022] and (c) complexes **26–27** [66] [adapted from ref. 66 with permission from the American Chemical Society, copyright 2024].

drug cisplatin, as confirmed by NMR spectroscopy through characteristic chemical shifts, indicating the encapsulation of two equivalents of cisplatin per cage molecule. This highlights the potential of these cages as host–guest systems. The scaffold containing the amide bond exhibits no cytotoxicity toward human A375 cells, further supporting its promise for application in drug delivery systems.

Jana *et al.* have synthesized and characterized four ternary Co(III) complexes featuring acetylacetonate-modified boron-dipyrromethene ligands (Fig. 4b). These complexes included $[Co(TPA)(L^1)](ClO_4)_2$ (**22**), $[Co(4\text{-}COOH\text{-}TPA)(L^1)](ClO_4)_2$ (**23**), $[Co(TPA)(L^2)]Cl_2$ (**24**), and $[Co(4\text{-}COOH\text{-}TPA)(L^2)]Cl_2$ (**25**), where L^1 represents acac-BODIPY and L^2 denotes acac-diiodo-BODIPY. The ligands TPA and 4-COOH-TPA refer to tris-(2-pyridylmethyl)amine and 2-((bis-(2-pyridylmethyl)amino)methyl) isonicotinic acid). These Co(III) complexes were assessed for their potential in bioimaging and phototherapeutic applications.[65] Single-crystal X-ray diffraction revealed a distorted octahedral geometry around the Co(III) centre in complex **11**. Bonding parameters in all 4 complexes were investigated using density function studies (DFT). Complexes **22** and **23** release an acac-BODIPY ligand upon photoactivation or in the presence of biological reducing agents, such as 3-mercaptopropionic acid, ascorbic acid, and glutathione (GSH). Ligand release was confirmed by enhanced emission intensity and corroborated by ^1H NMR spectroscopy. Among the series, complex **25**, containing a diiodo-BODIPY photosensitizer, exhibited the highest PDT activity with a phototherapeutic index (PI) exceeding 7000. It induces DNA photocleavage and generated both singlet oxygen ($^1O_2$) and superoxide radicals upon photoactivation. The localization study suggests that the green emissive complex **18** selectively accumulates in the endoplasmic reticulum of the A-549 lung carcinoma cells.

To address the poor photostability associated with iodinated ligand complexes, the study was further focused on designing new red light-activated photosensitizers based on non-iodinated ligands (Fig. 4c). Two heteroleptic Co(III) complexes, $[Co(TPA)\text{-}(L^1)](ClO_4)_2$ (**26**) and $[Co(TPA)(L^2)](ClO_4)_2$ (**27**), were synthesized.[66] These complexes incorporate a tetradentate polypyridyl ligand (TPA) along with an acetylacetone-linked PEGylated distyryl BODIPY ligand HL^1 and its dibromo analogue HL^2, respectively. The bromine-substituted BODIPY ligand enhances photodynamic therapy (PDT) by facilitating singlet oxygen generation through a type-II mechanism. Upon red light irradiation and under the reducing microenvironment typical of solid tumors, the Co(III) complexes undergo reduction to Co(II), triggering the release of the BODIPY photosensitizer. These complexes demonstrated excellent photophysical properties, mitochondrial targeting, strong fluorescence for imaging, and efficient singlet oxygen generation. Notably, complex **27** showed high photocytotoxicity against HeLa (cervical cancer) cells with minimal impact on normal cells, confirming its therapeutic selectivity. These findings offer a promising pathway for the development of red-light-responsive, biocompatible cobalt-based prodrugs for targeted cancer treatment.

Photodynamic therapy (PDT) relies on the generation of reactive oxygen species (ROS) to induce cytotoxic effects. However, its effectiveness is often limited by hypoxia, a common feature in solid tumors due to inadequate vascularization. The low oxygen levels hinder ROS production, reducing PDT efficacy and contributing to treatment resistance. To overcome the limitations imposed by tumor hypoxia, Zheng *et al.* have developed a near-infrared (NIR) photodynamic therapy (PDT) nanocomposite, DF–BODIPY@ZIF-8 (**28**).[67] The system combines a rationally designed BODIPY-based photosensitizer (DF–BODIPY) with a zeolitic imidazolate framework (ZIF-8) (Fig. 5a), which not only enhances singlet oxygen ($^1O_2$) generation through structural modulation (*e.g.*, trifluoromethyl substitution) but also catalyses the decomposition of endogenous hydrogen peroxide (H_2O_2) in tumors to generate oxygen, mitigating hypoxic conditions. Computational studies using density functional theory (DFT) demonstrated that the incorporation of more electronegative groups reduces the singlet–triplet energy gap (ΔE_{st}), promoting greater reactive oxygen species (ROS) generation. *In vitro* assessments under hypoxic conditions using 4T1 cancer cells demonstrated efficient cellular uptake of both DF–BODIPY and DF–BODIPY@ZIF-8, confirming their suitable particle size and biocompatibility. Further *in vivo* cytotoxicity studies in a 4T1 tumor-bearing mouse model revealed that DF–BODIPY@ZIF-8, upon 689 nm light irradiation, led to pronounced tumor growth inhibition.

As illustrated in (Fig. 5b) Chen *et al.* have designed and developed a novel PDT nanoplatform, 69-L_2@F (**29**), to address the persistent challenge of tumor hypoxia by combining fluorinated polyethylene glycol F-PEG with BODIPY-based zirconium metal–organic framework (Zr-MOF), 69-L_2.[68] They used a post-synthetic exchange method to successfully incorporate a carboxylated BODIPY ligand into a UiO-69-like MOF structure, forming the 69-L_2 framework. Further PEGylation with a fluorinated polymer resulted in the 69-L_2@F system, which enhances both oxygen solubility and biocompatibility. Owing to the oxygen-carrying capacity of the F-PEG, 69-L_2@F effectively alleviates hypoxia and facilitates reactive oxygen species (ROS) generation under LED light irradiation *in vitro*. The *in vivo* application, supported by a hydrogel-based delivery system, showed significant tumor suppression in a triple-negative breast cancer mouse model, MDA-MB-23. The 69-L_2@F-loaded hydrogel enables *in situ* oxygen generation and ROS production, offering effective tumor suppression.

Liang *et al.* have introduced an innovative NIR-responsive polymeric nanoplatform, termed NPIr@Bp (**30**), designed for targeted phototherapy (Fig. 5c).[69] The construction of this system involved synthesizing an amphiphilic polymer, PIr@Bp, by polymerizing a mitochondria-targeted Iridium(III) prodrug (Ir1) conjugated *via* a self-immolative linker to a BODIPY-based photosensitizer. To improve aqueous dispersibility and biocompatibility, polyethylene glycol (PEG) chains were introduced through terminal modification. In aqueous media, the resulting amphiphilic polymers self-assemble into gemini-type nanoparticles, forming NPIr@Bp, which can be selectively activated under near-infrared light irradiation. The

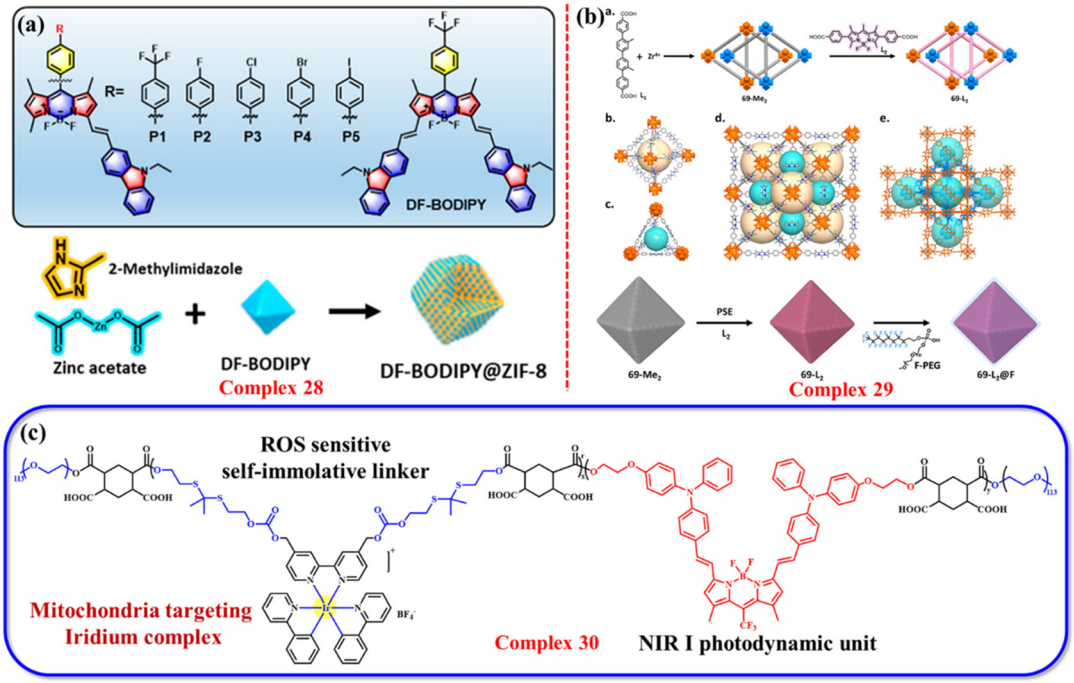

Fig. 5 (a) Structure of BODIPY photosensitizers and DF–BODIPY@ZIF-8 nanocomposite[67] [reproduced from ref. 67 with permission from the American Chemical Society, copyright 2022]. (b) Synthesis of zirconium-based MOFs for chemotherapeutic applications[68] [reproduced from ref. 68 with permission from the American Chemical Society, copyright 2024]. (c) Structure of an NIR-responsive amphiphilic polymeric prodrug (PIr@Bp)[69] [adapted from ref. 69 with permission from Elsevier, copyright 2024].

nanoparticle generating the singlet oxygen ($^1O_2$) upon irradiation was evaluated in a time-dependent manner by UV-Vis absorption spectroscopy. The nanoparticles show stability under physiological conditions and disassemble upon NIR irradiation to release the Ir(III) prodrug in a controlled manner. Cytotoxicity studies were conducted on human cervical carcinoma (HeLa) cells and cisplatin-resistant HeLa (HeLa–DDP) cells, showing an enhanced cytotoxic effect in the cisplatin-resistant cancer cells upon exposure to NIR irradiation. *In vitro* and *in vivo* studies, including RNA-seq analysis, confirmed the multimodal therapeutic mechanism and potent antitumor efficacy against cisplatin-resistant cancer models, highlighting the potential of platform for spatiotemporally controlled cancer therapy.

Bhattacharyya *et al.* have engineered a multi-ligand oxovanadium(IV)-β-diketonate prodrug having an NNN-donor, dipicolylamine conjugated to boron-dipyrromethene (BODIPY in L_1) and diiodo-BODIPY (in L_2) moieties, namely, [VO(L_1)(acac)]Cl (complex **31**), [VO(L_2)(acac)]Cl (complex **32**), and [VO(L_1)(dbm)]Cl (complex **33**), as shown in Fig. 6a, where acac and dbm are monoanionic O,O-donor acetylacetone and 1,3-diphenyl-1,3-propanedione.[70] The photo-induced cytotoxicity in HeLa cells was examined in visible light. The green emissive complex **31** and **33** are potent cellular imaging tools, while the non-fluorescent complex **32** is an efficient PDT agent, causing cellular apoptosis with a good photocytotoxic index (PI) value of >50 (IC_{50} in the dark: 58.0 μM; IC_{50} in the light: 1.1 μM). Jana *et al.* have engineered unique cobalt(III) dibromo-BODIPY-8-hydroxyquinolinate for mitochondria-targeted red light photodynamic therapy.[71] They synthesized three heteroleptic complexes with the general formula $[Co^{III}(L)(L_{1-3})]X$ (where X = ClO_4 for **34** and **35** and Cl for **36**) with tetradentate N,N,N,O-donor polypyridyl phenolate (**HL**) and bidentate N,O-donor 8-hydroxyquinoline ($\mathbf{HL_1}$) and its BODIPY ($\mathbf{HL_2}$) or dibromo-BODIPY ($\mathbf{HL_3}$) pendant ligands (Fig. 6b). The introduction of a monoanionic N,N,N,O-donor ancillary ligand has led to an improved bioavailability, and thereby enhanced therapeutic effect. The dibromo-BODIPY complex **34**, with a singlet oxygen quantum yield (ϕ_Δ) of ~0.25, exhibited remarkable apoptotic photo-cytotoxicity in HeLa cancer cells upon red light irradiation (600–720 nm), achieving a half-maximal inhibitory concentration (IC_{50}) in the nanomolar range (360 nM) and a photocytotoxicity index exceeding 277.

5.3. Curcumin-derived BODIPY metalloprodrugs

Curcumin, the active compound in turmeric which is also referred to as turmeric yellow, is a naturally occurring pigment renowned for its potential anti-cancer properties, a belief rooted in traditional Indian and Chinese medicine. However, clinical studies on the role of curcumin in cancer therapy have yielded mixed results. While it demonstrates potential as an adjunctive treatment in cancer therapy, its clinical application is hindered by challenges related to bioavailability and inconsistent evidence. Curcumin has shown improved physical performance in women with advanced breast cancer on intravenous administration of curcumin with paclitaxel chemo-

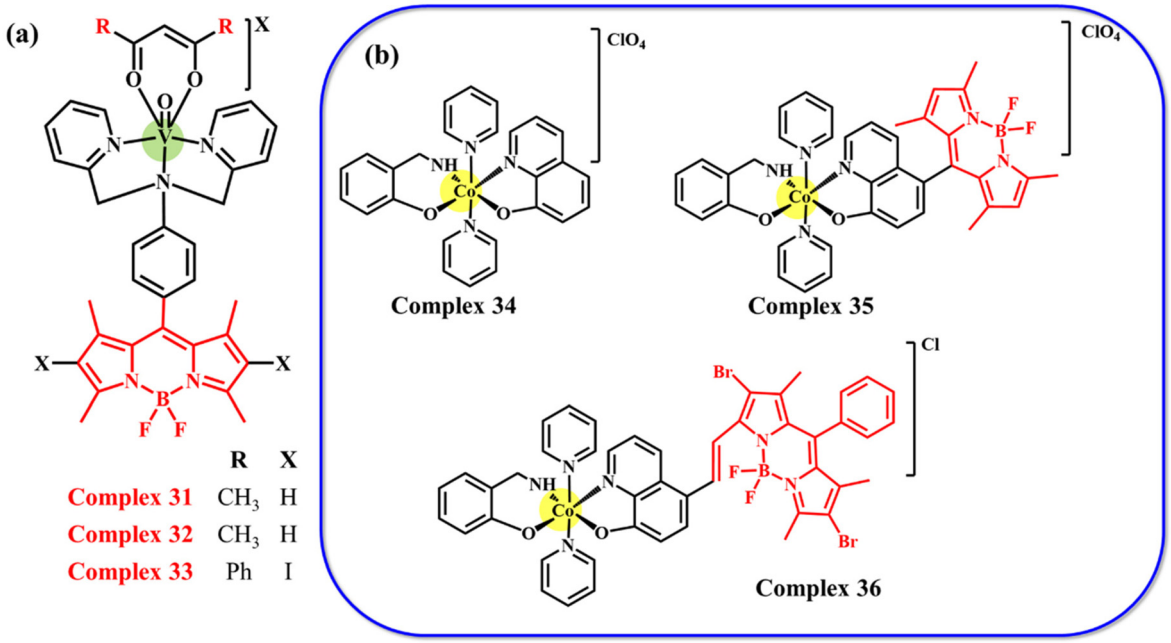

Fig. 6 Chemical structures of (a) oxovanadium-based[70] [adapted from ref. 70 with permission from the American Chemical Society, copyright 2020] and (b) cobalt-based complexes (**34–36**)[71] [adapted from ref. 71 with permission from Elsevier, copyright 2023].

therapy.[72] To enhance its bioavailability, researchers are exploring various delivery methods such as liposomal encapsulation, nanoparticle formulations, and co-administration with other adjuncts. Curcumin is typically known to generate hydroxyl radicals *via* the type-I PDT pathway. However, it exhibits poor bioavailability and is prone to hydrolysis under physiological conditions. Consequently, it has been recently categorized as pan-assay interference compound (PAINS) and invalid metabolic panaceas (IMPS) that obstructs the use of curcumin as a therapeutic agent in cancer management.[73]

Prof. Akhil Chakravarty and group have exclusively explored the conjugation of enolate form of curcumin with various metal ions, followed by its linkage to BODIPY dyes, to mitigate the undesirable characteristics associated with PAINS and IMPS.[74]

Addressing the aforementioned challenges, their research focuses on the designing of ternary oxidovanadium(IV) complexes (**37**) incorporating curcumin and dipicolylamine (dpa) ligands, along with analogues featuring pendant photoactive BODIPY moieties for cellular imaging (Fig. 7a).[75] These complexes exhibit visible light-induced cytotoxicity in breast and cervical cancer cells, leveraging the synergistic effects of metal coordination and photodynamic therapy. These emissive complexes were predominantly found to be localized in the mitochondria, inducing cellular apoptosis through the generation of singlet oxygen *via* the type-II photodynamic therapy (PDT) pathway. The mitochondrial localization of oxidovanadium complexes offers a strategic advantage over conventional cisplatin-based drugs, which majorly target the nucleus and are often hindered by intrinsic cellular resistance. VO^{2+} species further stabilizes curcumin, thereby retaining its therapeutic effect.

Visible light-activated photo-chemotherapeutic prodrug (**38**) was engineered by constructing ternary diamagnetic zinc(II) complexes of curcumin and dipicolylamine bases with a BODIPY photosensitizer (Fig. 7b).[76] Zinc, a redox inactive bioessential metal, exhibits low toxicity and strong coordination affinity with the enolate form of curcumin. Furthermore, it substantially enhances the stability of the di-iodinated BODIPY unit, thereby improving its physiological stability and fulfilling key pharmacological criteria necessary for effective drug actions.

Following a similar path, they further designed red-light-activated BODIPY-tagged platinum(II)–curcumin complexes with endoplasmic reticulum (ER) targeting ability (Fig. 7c).[77] By coordinating the enolate form of curcumin with platinum (II), these complexes achieve enhanced stability and bioavailability. The team synthesized and characterized non-iodo (RBC) (**39**) and di-iodinated (IRBC) (**40**) Pt complexes, each decorated with curcumin and N,N-donor 2-pyridylbenzimidazole ligands, and appended with red-light-responsive BODIPY pendants. These complexes were evaluated for their potential to induce red-light-mediated photodynamic therapy (PDT) effects. Upon evaluation against a non-BODIPY analogue, both RBC and IRBC exhibited significantly enhanced reactive oxygen species (ROS) generation. Surprisingly, the iodinated analogue (IRBC) demonstrated a unique mechanism by co-producing distinct types of ROS: hydroxyl radicals originating from the curcumin ligand and singlet oxygen ($^1O_2$) generated *via* the BODIPY moiety upon excitation with blue and red

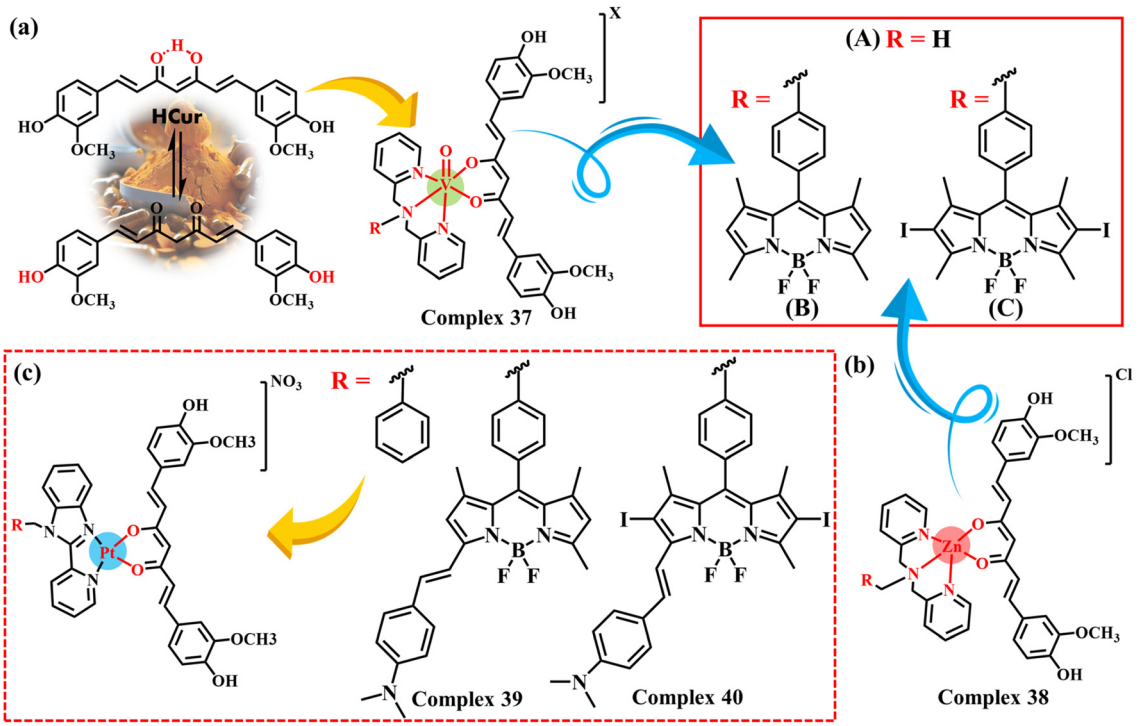

Fig. 7 Curcumin-based BODIPY-conjugated metalloprodrugs: (a) complex **37** [75] [adapted from ref. 75 with permission from the American Chemical Society, copyright 2027], (b) complex **38** [76] [adapted from ref. 76 with permission from Elsevier, copyright 2021] and (c) complex **39–40** [77] [adapted from ref. 77 with permission from the American Chemical Society, copyright 2022].

light, respectively. These complexes also exhibited potent photoinduced cytotoxicity across a broad spectral range.

5.4. Biotin targeting metalloprodrugs

A widely used approach to enhance the selectivity and efficacy of photodynamic therapy (PDT) agents toward tumors involves conjugating the photosensitizer with tumor-targeting compounds, namely vitamins, folic acid, peptides, and steroids.[78] This strategy ensures that the photosensitizer, functioning as a prodrug, is selectively directed to cancer cells. Among these targeting ligands, biotin, also known as vitamin H, has gained significant attention due to its essential role in various metabolic processes and its association with the rapid proliferation of cancer cells. The high metabolic demand of these rapidly dividing cells leads to a markedly increased biotin uptake in many tumor types. This phenomenon is primarily driven by the overexpression of biotin-specific receptors and transporters on the surface of cancer cells, such as the sodium-dependent multivitamin transporter (SMVT).[79] Consequently, biotin serves as an effective targeting ligand for tumor-specific delivery of therapeutic agents, including PDT prodrugs.

As displayed in Fig. 8, Akhil R. Chakravarty and coworkers have designed 5 ruthenium(II) complexes (**41–45**) incorporating BODIPY as a photoactive dye and biotin for targeted photodynamic therapy (PDT). The five mixed ligand complexes were designed for PDT in the presence of red light based on ruthenium(II) coordinating with different ligands including NNN-donor dipicolylamine (dpa) bases (L_4, L_5), NN-donor phenanthroline derivatives (L_1, L_2), and benzyldipicolylamine (bzdpa, L_3).[80] These complexes exhibit strong luminescence properties, making them suitable for cellular imaging and function as efficient photosensitizers under visible (400–700 nm) and near-infrared (600–720 nm) light. The complexes exhibit mitochondrial localization, which may lead to apoptotic cell death. The ROS here is a singlet oxygen ($^1O_2$) generated through the type II PDT pathway, as evident from the mechanistic DNA photocleavage study. The BODIPY Ru(II) complex containing biotin and PEG pendant groups exhibited significant PDT activity under red light irradiation (600–720 nm) in human lung carcinoma A549 cells. The A549 cell line was selected due to its known overexpression of SMVT receptors. The biotinylated derivative exhibits superior photocytotoxicity relative to its non-biotinylated counterpart due to enhanced cellular uptake mediated by biotin receptor-targeting mechanisms.

Paul *et al.* have developed biotin-decorated BODIPY–ruthenium(II) bis-terpyridine complexes (**46**) displaying an ultra-high phototherapeutic index of >1400 (Fig. 9a). The complex generated singlet oxygen species ($^1O_2$) *via* a type-II mechanism and superoxide anion radicals (O_2^-) through a type-I pathway upon photoexcitation. $^1O_2$ causes cellular apoptosis while O_2^- aids in DNA cleavage. It exhibited excellent phototoxicity against human cervical cancer cell lines (HeLa).[81]

A. Bera *et al.* synthesized a Pt(IV) prodrug, *cis*,*cis*,*trans*-[Pt$(NH_3)_2Cl_2$(biotin)(L)] (**47**), derived from cisplatin. The prodrug

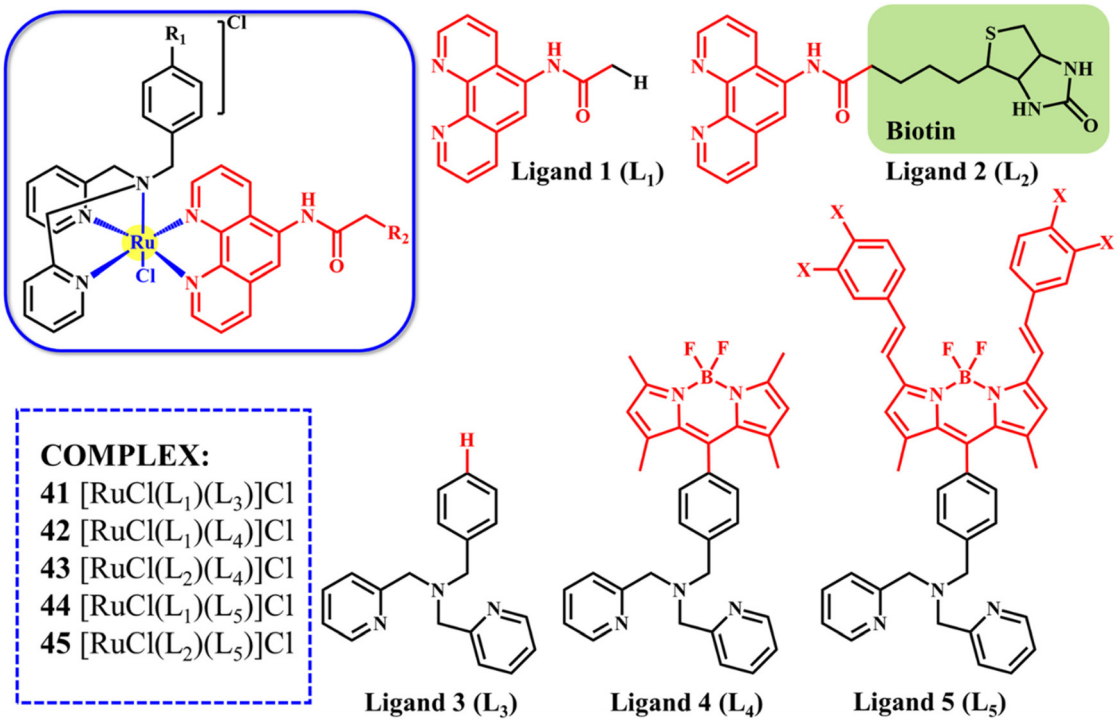

Fig. 8 Chemical structures of Ru(II) complexes[80] [adapted from ref. 80 with permission from the American Chemical Society, copyright 2020].

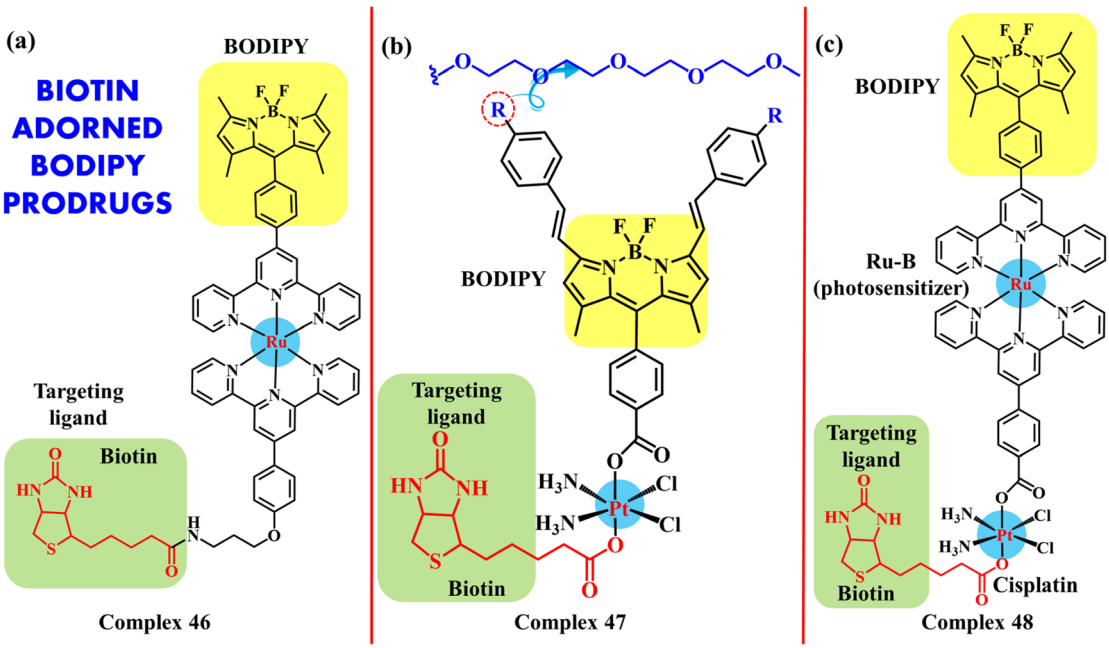

Fig. 9 Biotin-adorned BODIPY-conjugated (a) ruthenium-based[81] [adapted from ref. 81 with permission from the American Chemical Society, copyright 2021], (b) platinum-based PEGylated[82] [adapted from ref. 82 with permission from the Royal Society of Chemistry, copyright 2023] and (c) ruthenium–platinum bimetallic prodrugs[83] [adapted from ref. 83 with permission from the American Chemical Society, copyright 2024].

features a *cis*,*cis*,*trans*-configured Pt(IV) core, incorporating an axial biotin ligand for cancer-targeted delivery and a PEGylated BODIPY photosensitizer (HL) responsive to red light (Fig. 9b).[82] The prodrug strategy enhances the photocytotoxicity of platinum-based PDT by exploiting a chemo-PDT mechanism, enabling selective targeting of cancer cells over normal tissues. Upon red-light irradiation, the system undergoes one-step, two-electron photoreduction of the Pt(IV) centre, releasing

an active cisplatin analogue alongside the PDT-active BODIPY photosensitizer. Notably, the intact Pt(IV) complex also contributes to PDT efficacy due to the coordinated BODIPY moiety. The BODIPY ligand functions as an efficient red-light-activated photosensitizer, generating singlet oxygen as the primary reactive oxygen species (ROS) in high yields (Table 2). The biotin- and PEGylated distyryl-BODIPY-conjugated complex demonstrated significantly enhanced cellular uptake in A549 cancer cells compared to non-cancerous Beas-2B cells, as confirmed by flow cytometry. This dual-action therapeutic approach combining photodynamic and chemotherapeutic modalities holds promise for overcoming drug resistance and enhancing the precision and potency of cancer treatment.

The group further developed a "magic bullet" for the targeted drug delivery and developed a heterobimetallic Pt(IV)–Ru(II) complex, *cis*,*cis*,*trans*-[$Pt(NH_3)_2Cl_2${Ru(tpy-BODIPY)(tpy-COO)}(biotin)]Cl_2 (Pt–Ru–B, 2) (**48**) (Fig. 9c). In this system, the pseudo-octahedral $5d^6$-Pt(IV) centre is axially coordinated to biotin and a Ru(II) photosensitizer complex, {Ru(II)-tpy-BODIPY} (Ru–B, 1) (**49**). The Ru–B unit features a BODIPY-based photosensitizer bonded to a nitrogen-donor tpy (4′-phenyl-2,2′:6′,2″-terpyridine) ligand.[83] This dual-functional complex is designed as a "Platin Bullet" for targeted photodynamic therapy (PDT), combining selective tumor targeting through the biotin moiety and efficient reactive oxygen species (ROS) generation *via* the Ru–B photosensitizer upon light activation. This multifunctional molecular platform demonstrates efficient cellular uptake, facilitated by the biotin moiety. Upon light activation, the Ru(II)-based photosensitizer efficiently generates singlet oxygen ($^1O_2$) as the predominant reactive oxygen species (ROS), with a minor contribution from superoxide anion radicals through a type-I electron transfer pathway. Complex **48** (Pt–Ru–B) exhibits pronounced mitochondrial localization and induces light-triggered apoptotic cell death, demonstrating an exceptional photocytotoxicity index exceeding 4500. The scratch-wound healing assay performed on A549 cells revealed that the Pt–Ru–B prodrug complex effectively inhibits cell migration, indicating its potential antimetastatic activity.

6. Other biological applications of BODIPY–metal conjugates

Recent advances in BODIPY–metal systems have greatly expanded the applications of these dyes beyond anticancer phototherapy, especially in sensing and imaging of biologically and environmentally relevant metal ions. A prominent example is the NIR–BODIPY derivative "BPN" which exhibits emission at 765 nm (upon excitation at 704 nm) and shows distinct responses towards Cu^{2+} and Mn^{2+}, wherein binding to Cu^{2+} causes quenching of emission, while Mn^{2+} induces aggregation and fluorescence enhancement. BPN has been successfully used to monitor Cu^{2+} in live cells and image the mitochondria, and its detection range in the serum spans ≈0.45 μM to 36.30 μM.[84] BODIPY-based sensors have also been developed in hydrogel formulation. A fluorescent dialdehyde-BODIPY cross-linked chitosan hydrogel (CBC) has been shown to identify Cu^{2+} in aqueous solutions, with a linear quenching response up to ~50 μM, a detection limit of ≈4.75 μM, and a quenching constant of ~3.52×10^4 M^{-1}. The mechanism involves Cu^{2+}-triggered conversion of imine (C=N) bonds in the hydrogel moiety.[85] In another study, an asymmetric BODIPY sensor functionalized with a bis(pyridine-2-ylmethyl)amine group and a 4-carboxyphenyl substituent was used for ratiometric sensing of Cu^{2+}. Upon binding, the fluorescence emission peak shifts from ~580 nm to ~620 nm; the binding stoichiometry is ~1 : 3 (BODIPY : Cu^{2+}), and the ratio of emission intensities at 620 nm *vs.* 580 nm (F_{620}/F_{580}) increases with the Cu^{2+} concentration. This enables naked-eye detection in aqueous samples.[86]

Mondal, Majee, and Dutta (2025) have developed a BODIPY-based *N*-oxide probe (BDNO) that exhibits ratiometric near-infrared fluorescence when detecting ferrous ions (Fe^{2+}). BDNO displays a dual emission behavior: a "turn-off" emission at ~570 nm under excitation at ~540 nm, and a strong "turn-on" NIR emission at approx. 715 nm (excitation ~610 nm), with a large Stokes shift (~105 nm). The detection limit is about 41 nM, and the probe works in <5 seconds in real sample matrices such as fruit juices, tap water, and river water, specifically useful in applications in food safety, environmental monitoring, and biomedical research.[87]

Emerging studies further indicate that BODIPY dyes are highly promising for tackling bacterial infections using photodynamic methods and other antibacterial approaches. For example, Wen *et al.* (2023) designed several functionalized BODIPYs bearing groups such as phenylboronic acid (PBA) or pyridine cations; one of the derivatives (IBDPPy–Ph) not only efficiently killed *Staphylococcus aureus* and *Escherichia coli* under illumination, but also eradicated mature biofilms and promoted wound healing in infected models.[88] Similarly, Li, Li, Wu, Sun & Xie *et al.* reported a BODIPY photosensitizer, LIBDP, containing a guanidine moiety, which disrupts bacterial membranes, generates reactive oxygen species under light, destroys preformed biofilms, and also, through ROS-mediated oxidation of the guanidine, releases nitric oxide that aids wound healing.[45] In another line, BODIPY@carbon dot nanocomposites (positively charged) have been shown to exhibit extremely low minimal inhibitory concentrations (MICs) against *S. aureus* (as low as ~128 ng mL^{-1}) and to accelerate the healing of bacterial infections in wound models.[89] The inclusion of heavy atoms such as iodine has also been exploited: a study comparing several BODIPY derivatives found that 2,6-diiodo-8-phenyl-substituted BODIPY (BDP3) killed *S. aureus* at MIC ~10 nM under green–light irradiation, with good biofilm inhibition and favorable cytocompatibility.[90] Moreover, cationic BODIPY derivatives (including dicationic aza-BODYPS) have shown potent activity against clinical and antibiotic resistant strains of MRSA upon illumination; for instance, one such compound achieved minimum bactericidal concentrations in the range of ~12.5–25 μM for many strains.[91] Moreover, BODIPY conjugated with triphenylphosphine (BDPI–TPP) when formed into nanoparticles shows

Table 2 Comparative summary of light-activated prodrugs and their photodynamic performances

Sr. no.	Metal (Ox. state)	Ligand/system	Light	ROS	PDT pathway	Cell line(s)	IC_{50} light (μM)	IC_{50} Dark (μM)	Targeting/accumulation	Ref.
Platinum-based BODIPY prodrugs										
1	Pt(IV)	Carbamate, triazole linkers	Blue	Cisplatin release	–	MCF-7	Low μM	Non-toxic	Cytoplasm	50
2	Pt(IV)	Carboplatin	Green	$^1O_2$, $O_2^{\bullet-}$	II + I	MCF-7 SKOV3	15.7 22.4	173.4 >200	Cytoplasm, DNA	51
3	Pt(IV)	Hydroxido/acetato	White	$OH^{\bullet}$, $O_2^{\bullet-}$	I	A2780	43.8	>100	Cytoplasm	52
4	Pt(IV)	Distyryl-dibromo-BODIPY	NIR	$OH^{\bullet}$, $O_2^{\bullet-}$	I	MCF-7 VA-13	1.7 ± 0.1 6.1 ± 0.4	>20 >20	Cytoplasm	53
5	Pt(IV)	BODIPY	—	—	—	HeLa MCF-7	27.37 12.14	— —	Mitochondria	54
6	Pt(II)	Pyriplatin–BODIPY (3 iodo variants)	Visible	$^1O_2$	II	A549 MCF-7 HaCaT	0.05–1.7 0.07–0.40 0.06–1.0	73.2–>100	Mitochondria	55
7	Pt(IV)	Oxoplatin-B–BODIPY	Visible	$^1O_2$	II	MCF-7, HeLa, A549	1.1–3.8	—	Mitochondria	56
8	Pt(II)	Maloplatin-B (styryl BODIPY)	NIR-red	$^1O_2$	II	A549, HeLa	1.6–2.4	—	Mitochondria	57
9	Pt(IV)	—	Red	$^1O_2$	II	HeLa, MCF-7	0.58–0.76	—	Mitochondria, ER	58
10	Pt(IV)	Sulfonamide (Bodi–Car–ER)/morpholine (Bodi–Car–Ly)/PPh_3 (Bodi–Car–Mt)	Green	$^1O_2$	II	A549 A549cisR A2780 A2780cisR HeLa HepG2	35.7/65.7/20.5 40.2/75.7/22.6 9.4/28.3/11.1 38.9/67.1/8.3 26.7/63.1/38.9 9.5/21.4/9.7	>80/>160/>113.5 >80/>160/>160 >80/43.4/16.9 >80/152.2/24.8 147/>160/>80 16.9/>160/>160	ER, lysosome, mitochondria	59
11	Pt(II)	Glycosylated BODIPY	Visible	$^1O_2$	II	HT29 A549 R-HepG2	0.42 0.56 0.59	— — —	GLUT1-mediated	60
12	Pt(II)	Terpyridine (tpy), glucose-appended tpy, 8-(4-ethynylphenyl)-distyryl-BODIPY	Red	$^1O_2$	II	HeLa MCF-7 A549	2.3–24.7	>100	Mitochondria, glucose transporter	63
Other-metal based BODIPY prodrugs										
13	Pd(II)	3,5-Bis(3-ethynylpyridine) phenyl	—	—	—	A375	EC_{50} > 50	—	Mitochondria	64
14	Co(III)	TPA (**22**), 4-COOH–TPA (**23**), acac-BODIPY (**24**), acac-diiodo BODIPY (**25**)	Visible	$^1O_2$ $O_2^{\bullet-}$	II I	HeLa	Complex **25**: 0.007	—	Endoplasmic reticulum	65
15	Co(III)	TPA, acac-linked PEGylated distyryl BODIPY and dibromo derivative	Red	$^1O_2$	II	HeLa	0.23	—	Mitochondria	66
16	Zn (ZIF-8)	—	NIR	$^1O_2$	II	4T1	Not specified; stronger effect *vs.* free DF–BODIPY	—	Hypoxic TME (passive targeting)	67
17	Zr-MOF	—	LED	ROS	—	MDA-MB-231	—	—	TME (oxygen carrier)	68
18	Ir(III)	Thiol-modified bipyridine	NIR	$^1O_2$	II	HeLa	1.3 ± 0.2	>100	Mitochondria	69
19	V(IV)	BODIPY and diiodo-BODIPY β-diketonates (complexes **31**–**33**)	Visible	$^1O_2$	II	HeLa	12.5/1.1/6.3	>100	Mitochondria	70
20	Co(III)	Dibromo-BODIPY-8-hydroxyquinoline (complex **26**/**27**)	Red	$^1O_2$	II	HeLa A549	5.44/0.36 7.40/0.52	>100 >100	Mitochondria	71
Curcumin-based BODIPY metalloprodrugs										
21	VO^{2+}	Dipicolylamine (dpa), diiodo-BODIPY (complexes **37** a/b/c)	Visible	$OH^{\bullet}$ $^1O_2$	I II	HeLa MCF-7	15.5 ± 0.9/5.8 ± 0.5/2.5 ± 0.2 8.8 ± 0.4/6.2 ± 0.2/2.7 ± 0.4	>100/>100/55 ± 2 94 ± 2/87 ± 2/99 ± 3	Mitochondria	75
22	Zn(II)	Dipicolylamine (dpa), diiodo-(complexes **38** a/b/c)	Visible	$OH^{\bullet}$ $^1O_2$	I II	HeLa MCF-7	6.1 ± 0.2/1.0 ± 0.1/0.025 ± 0.007 8.0 ± 0.1/1.4 ± 0.1/0.055 ± 0.01	58.4 ± 0.2/48.8 ± 0.7/64.6 ± 0.2 61.8 ± 0.3/48.7 ± 0.2/71.0 ± 0.3	Mitochondria	76

Table 2 *(Contd.)*

Sr. no.	Metal (Ox. state)	Ligand/system	Light	ROS	PDT pathway	Cell line(s)	IC_{50} light (μM)	IC_{50} Dark (μM)	Targeting/accumulation	Ref.
23	Pt(II)	N,N-Donor 2-pyridylbenzimidazole (RBC/IRBC)	Blue	$OH^{\bullet}$	II	A549	4.5 ± 0.1/1.3 ± 0.4	56.2 ± 0.1/53.9 ± 0.3	Endoplasmic reticulum	77
			Red	$^1O_2$		HeLa	5.0 ± 0.1/2.4 ± 0.1	52.4 ± 0.3/56.4 ± 0.1		
						MDA-MB-231	6.9 ± 0.1/2.4 ± 0.1	57.3 ± 0.6/49.6 ± 0.8		
Biotin-based										
24	Ru(II)	Dpa, phenanthroline derivative, bzdpa	Red	$^1O_2$	II	A549	Complex **44:** 0.04; complex **45:** 0.02	>100	Mitochondria	
25	Ru(II)	tpy-BODIPY, tpy-biotin (complex **46**)	Visible	$^1O_2$	II	A549	0.16	>100	Biotin-mediated uptake, cytosolic localization	
				$O_2^{\bullet-}$	I	HeLa	0.07			
26	Pt(IV)	PEGylated distyryl-BODIPY	Red	$^1O_2$	II	A549	0.61–1.54	>100	Mitochondria	
						MDA-MB-231				
27	Ru(II) Pt(IV)	tpy-BODIPY, tpy-COO	Red	$^1O_2$, $O_2^{\bullet-}$	II I	A549	0.022	>100	Mitochondria	
						MDA-MB-231	0.050			

strong electrostatic binding to bacterial membranes and effective photodynamic antibacterial activity with low MIC (~0.3 μg mL^{-1}) against typical bacterial pathogens.[92] Finally, approaches have extended beyond planktonic bacteria: covalent attachment of a BODIPY derivative (with a heavy atom for enhanced singlet–oxygen generation) to a polymeric surface (*e.g.* PDMS) yielded antimicrobial surfaces that significantly reduced *Staphylococcus aureus* colonization under light exposure.[93]

7. Conclusion and future perspectives

This review elaborates the advances in metallo-prodrugs adorned with boron dipyrromethene derivatives (BODIPY) taking on a dual role as a chemotherapeutic and PDT agent. Cisplatin remains a cornerstone of cancer therapy, and researchers have built upon it to develop newer drugs with advanced features such as target specificity and bioimaging capabilities. One of the first approaches to address the limitations of cisplatin was to design Pt(IV) prodrugs as kinetically inert derivatives that reduce off-target reactivity and toxicity by activating only within cancer cells. More recently, BODIPY-conjugated prodrugs have emerged, combining therapeutic action with intrinsic fluorescence for real-time bioimaging. Later, scientists explored the potency of other metals such as ruthenium (Ru), cobalt (Co) and vanadium(V). These provided safer options as compared to platinum-based drugs. Subsequently, prodrugs were engineered with targeting ligands such as biotin and designed for organelle-specific delivery, specifically mitochondrial targeting, to overcome the demerits of nuclear-targeted conventional metallodrugs. A group of researchers are actively researching on combining the goodness of the golden spice 'curcumin' and the fluorescence of BODIPY with metalloprodrugs, and these hybrid constructs have shown promising anticancer activity.

Substantial efforts have focused on transforming metal-based drugs into prodrugs to enhance their therapeutic efficacy and overcome inherent limitations. Although cisplatin derivatives remain the most extensively studied metallodrugs for cancer therapy, several promising avenues remain relatively uncharted. Even though investigations into other transition metals such as Pd, Co, Ru, and V have begun offering new action mechanisms, the first-row transition metals such as copper and iron remain significantly underexplored. They provide alternative pathways to the conventional DNA targeting such as angiogenesis, cuproplasia, cuproptosis and ferroptosis, opening better and safer opportunities.

Researchers are deep diving into the benefits of nanoformulating drugs to improve solubility, targeting precision, and controlled release. As outlined in this review, early-stage efforts are exploring the conjugation of metalloprodrugs into nanoformulations. While still in its infancy, this strategy holds significant potential to harness the benefits of metallotherapeutics while mitigating their drawbacks. Much deeper assessment is required to package more features such as stimuli response, deep tissue activation and advanced protein targeting. In conclusion, integrating BODIPY into metalloprodrugs has

unlocked novel chemotherapeutic strategies offering bioimaging and photodynamic capabilities and enhanced selectivity, yet much remains to be explored in designing smarter and multifunctional drugs.

Author contributions

Twara Kikani: Investigation, formal analysis, methodology, writing – review & editing, and visualization. Krutika Patel: Formal analysis and validation. Sonal Thakore: Conceptualization, supervision, project administration, data curation, writing – review & editing, and funding acquisition.

Conflicts of interest

The authors report no declarations of interest.

Data availability

No primary research results, software or code have been included and no new data were generated or analysed as part of this review.

Acknowledgements

The authors are grateful to DST-SERB Power Grant (SPG/2021/0003149) and Gujarat State Biotechnology Mission (GSBTM/JD(R&D)/663/2023-24/02636616) for financial assistance.

References

1 A. M. Itoo, M. Paul, S. G. Padaga, B. Ghosh and S. Biswas, *ACS Omega*, 2022, **7**, 45882–45909.
2 A. Zafar, S. Khatoon, M. J. Khan, J. Abu and A. Naeem, *Discover Oncol.*, 2025, **16**.
3 L. Zhang, H. Chen, Z. Jiang, Z. Xu, Y. Gao, Y. Gao, Y. Liang, Q. Li, H. Lan, M. Liu, Y. Li and B. Zhao, *Chem. Eng. J.*, 2025, **505**, 159096.
4 J. H. Chen, J. V. Lim and Y. C. Hsu, *NanoTrends*, 2025, **9**, 100084.
5 S. Duan, Y. Hu, Y. Zhao, K. Tang, Z. Zhang, Z. Liu, Y. Wang, H. Guo, Y. Miao, H. Du, D. Yang, S. Li and J. Zhang, *RSC Adv.*, 2023, **13**, 14443–14460.
6 Y. A. Martins, T. Z. Pavan and R. F. V. Lopez, *Int. J. Pharm.*, 2021, **610**, 121243.
7 F. Gao, F. Gao, W. J. Zhang, C. Y. Hong, Y. Z. You, X. Nie, Z. Zhang, G. Chen, L. Xia, L. H. Wang, W. J. Zhang, C. Y. Hong, Y. Z. You, F. Wang, C. H. Wang and Z. Y. Hao, *New J. Chem.*, 2020, **44**, 3478–3486.
8 A. S. Casabianca, V. Tsagkalidis, P. R. Burchard, A. Chacon, A. Melucci, A. Reitz, D. A. Swift, A. A. McCook, J. M. Switchenko, M. M. Shah and D. R. Carpizo, *Eur. J. Surg. Oncol.*, 2022, **48**, 2448–2454.
9 C. Holohan, S. Van Schaeybroeck, D. B. Longley and P. G. Johnston, *Nat. Rev. Cancer*, 2013, **13**, 714–726.
10 B. Farhood, K. Mortezaee, E. Motevaseli, H. Mirtavoos-Mahyari, D. Shabeeb, A. E. Musa, N. S. Sanikhani, M. Najafi and A. Ahmadi, *J. Cell. Biochem.*, 2019, **120**, 18559–18571.
11 W. Zhao, L. Wang, M. Zhang, Z. Liu, C. Wu, X. Pan, Z. Huang, C. Lu and G. Quan, *MedComm*, 2024, **5**, 1–36.
12 A. M. Oluwajembola, W. D. Cleanclay, A. F. Onyia, B. N. Chikere, S. Zakari, E. Ndifreke and O. C. De Campos, *Results Chem.*, 2024, **10**, 101715.
13 A. Escudero, C. Carrillo-Carrión, M. C. Castillejos, E. Romero-Ben, C. Rosales-Barrios and N. Khiar, *Mater. Chem. Front.*, 2021, **5**, 3788–3812.
14 Y. Tang, L. Xue, Q. Yu, D. Chen, Z. Cheng, W. Wang, J. Shao and X. Dong, *ACS Appl. Bio Mater.*, 2019, **2**, 5888–5897.
15 L. Maierhofer, R. Prieto-Montero, T. Cubiella, A. Díaz-Andrés, N. Morales-Benítez, D. Casanova, V. Martínez-Martínez, M. D. Chiara, E. Mann and J. L. Chiara, *J. Mater. Chem. B*, 2025, **13**, 4330–4340.
16 J. Wang, W. Li, L. Jiao and E. Hao, *Chem. Commun.*, 2025, **61**, 4465–4482.
17 A. C. Scanone, S. C. Santamarina, D. A. Heredia, E. N. Durantini and A. M. Durantini, *ACS Appl. Bio Mater.*, 2020, **3**, 1061–1070.
18 P. Kaur and K. Singh, *J. Mater. Chem. C*, 2019, **7**, 11361–11405.
19 M. K. Raza, S. Gautam, A. Garai, K. Mitra, P. Kondaiah and A. R. Chakravarty, *Inorg. Chem.*, 2017, **56**, 11019–11029.
20 H. Martin, L. R. Lázaro, T. Gunnlaugsson and E. M. Scanlan, *Chem. Soc. Rev.*, 2022, **51**, 9694–9716.
21 G. Zhang, Y. Zhu, Y. Wang, D. Wei, Y. Wu, L. Zheng, H. Bai, H. Xiao and Z. Zhang, *RSC Adv.*, 2019, **9**, 20513–20517.
22 R. Ni, J. Zhu, Z. Xu and Y. Chen, *J. Mater. Chem. B*, 2020, **8**, 1290–1301.
23 M. Das, A. Joshi, R. Devkar, S. Seshadri and S. Thakore, *Bioconjugate Chem.*, 2022, **33**, 369–385.
24 H. Chen, T. Sun, W. Zeng, X. Zeng, L. Mei, C. Jiang and Y. Zhao, *ACS Mater. Lett.*, 2022, **4**, 111–119.
25 D. Chen, Y. Tang, J. Zhu, J. Zhang, X. Song, W. Wang, J. Shao, W. Huang, P. Chen and X. Dong, *Biomaterials*, 2019, **221**, 119422.
26 S. Adhikari, P. Nath, A. Das, A. Datta, N. Baildya, A. K. Duttaroy and S. Pathak, *Biomed. Pharmacother.*, 2024, **171**, 116211.
27 A. Polavarapu, J. A. Stillabower, S. G. W. Stubblefield, W. M. Taylor and M.-H. Baik, *J. Org. Chem.*, 2012, **77**, 5914–5921.
28 J. A. O. Rodrigues, N. S. Kiran, A. Chatterjee, B. G. Prajapati, N. Dhas, A. O. dos Santos, F. F. de Sousa and E. B. Souto, *Biochem. Pharmacol.*, 2025, **231**, 116644.
29 M. Maji, S. Karmakar, Ruturaj, A. Gupta and A. Mukherjee, *Dalton Trans.*, 2020, **49**, 2547–2558.
30 J. Shum, P. K. K. Leung and K. K. W. Lo, *Inorg. Chem.*, 2019, **58**, 2231–2247.

31 T. Chen, Z. Xiao, X. Liu, T. Wang, Y. Wang, F. Ye, J. Su, X. Yao, L. Xiong and D. H. Yang, *Pharmacol. Res.*, 2024, **202**, 107099.
32 M. J. Chow, C. Licona, G. Pastorin, G. Mellitzer, W. H. Ang and C. Gaiddon, *Chem. Sci.*, 2016, **7**, 4117–4124.
33 S. Movassaghi, E. Leung, M. Hanif, B. Y. T. Lee, H. U. Holtkamp, J. K. Y. Tu, T. Söhnel, S. M. F. Jamieson and C. G. Hartinger, *Inorg. Chem.*, 2018, **57**, 8521–8529.
34 R. K. Singh, S. Kumar, D. N. Prasad and T. R. Bhardwaj, *Eur. J. Med. Chem.*, 2018, **151**, 401–433.
35 Z. Zhao, X. Zhang, C. E. Li and T. Chen, *Biomaterials*, 2019, **192**, 579–589.
36 E. J. Anthony, E. M. Bolitho, H. E. Bridgewater, O. W. L. Carter, J. M. Donnelly, C. Imberti, E. C. Lant, F. Lermyte, R. J. Needham, M. Palau, P. J. Sadler, H. Shi, F. X. Wang, W. Y. Zhang and Z. Zhang, *Chem. Sci.*, 2020, **11**, 12888–12917.
37 L. Kelland, *Nat. Rev. Cancer*, 2007, **7**, 573–584.
38 R. Oun, Y. E. Moussa and N. J. Wheate, *Dalton Trans.*, 2018, **47**, 6645–6653.
39 S. Thota, D. A. Rodrigues, D. C. Crans and E. J. Barreiro, *J. Med. Chem.*, 2018, **61**, 5805–5821.
40 C. Santini, M. Pellei, V. Gandin, M. Porchia, F. Tisato and C. Marzano, *Chem. Rev.*, 2014, **114**, 815–862.
41 D. Mahendiran, S. Amuthakala, N. S. P. Bhuvanesh, R. S. Kumar and A. K. Rahiman, *RSC Adv.*, 2018, **8**, 16973–16990.
42 C. R. Munteanu and K. Suntharalingam, *Dalton Trans.*, 2015, **44**, 13796–13808.
43 F. H. Quina and G. T. M. Silva, *J. Photochem. Photobiol.*, 2021, **7**, 100042.
44 J. An, S. Tang, G. Hong, W. Chen, M. Chen, J. Song, Z. Li, X. Peng, F. Song and W. H. Zheng, *Nat. Commun.*, 2022, **13**, 1–10.
45 C. Li, Y. Li, Q. Wu, T. Sun and Z. Xie, *Biomater. Sci.*, 2021, **9**, 7648–7654.
46 R. Wang, X. Li and J. Yoon, *ACS Appl. Mater. Interfaces*, 2021, **13**, 19543–19571.
47 D. Wang and S. J. Lippard, *Nat. Rev. Drug Discovery*, 2005, **4**, 307–320.
48 S. Ghosh, *Bioorg. Chem.*, 2019, **88**, 102925.
49 C. Tang, M. J. Livingston, R. Safirstein and Z. Dong, *Nat. Rev. Nephrol.*, 2023, **19**, 53–72.
50 D. Spector, A. Bubley, A. Zharova, V. Bykusov, D. Skvortsov, D. Ipatova, A. Erofeev, P. Gorelkin, A. Vaneev, D. Mazur, V. Nikitina, M. Melnikov, V. Pergushov, D. Bunin, V. Kuzmin, A. Kostyukov, A. Egorov, E. Beloglazkina, R. Akasov and O. Krasnovskaya, *ACS Appl. Bio Mater.*, 2024, **7**, 3431–3440.
51 H. Yao, S. Chen, Z. Deng, M. K. Tse, Y. Matsuda and G. Zhu, *Inorg. Chem.*, 2020, **59**, 11823–11833.
52 H. Yao, Y. F. Gunawan, G. Liu, M. K. Tse and G. Zhu, *Dalton Trans.*, 2021, **50**, 13737–13747.
53 D. V. Spector, V. Bykusov, A. Zharova, I. Kuzmichev, Y. A. Isaeva, E. V. Khaydukov, E. Trifanova, M. Stepanov, A. S. Erofeev, P. Gorelkin, R. Kuanaeva, V. N. Nikitina, A. Dubenskii, Y. Maksimova, D. A. Skvortsov, D. Ipatova, I. A. Rodin, M. F. Vokuev, A. G. Martynov, D. Bunin, V. S. Pokrovsky, G. Babayeva, T. Uskova, M. A. Abakumov, E. K. Beloglazkina, R. A. Akasov and O. O. Krasnovskaya, *ACS Appl. Nano Mater.*, 2024, **7**, 25603–25618.
54 T. Sun, X. Guan, M. Zheng, X. Jing and Z. Xie, *ACS Med. Chem. Lett.*, 2015, **6**, 430–433.
55 M. K. Raza, S. Gautam, P. Howlader, A. Bhattacharyya, P. Kondaiah and A. R. Chakravarty, *Inorg. Chem.*, 2018, **57**, 14374–14385.
56 A. Bera, S. Gautam, M. K. Raza, P. Kondaiah and A. R. Chakravarty, *J. Inorg. Biochem.*, 2021, **223**, 111526.
57 V. Ramu, P. Kundu, P. Kondaiah and A. R. Chakravarty, *Inorg. Chem.*, 2021, **60**, 6410–6420.
58 A. Bera, S. Gautam, S. Sahoo, A. K. Pal, P. Kondaiah and A. R. Chakravarty, *RSC Med. Chem.*, 2022, **13**, 1526–1539.
59 Y. Xu, F. Zhang, M. Li, H. Zhang, Y. Yuan, S. Lin, L. Yao, S. Xu, T. Yuan and H. Yao, *Dalton Trans.*, 2025, **54**, 5849–5858.
60 G. Durán-Sampedro, E. Y. Xue, M. Moreno-Simoni, C. Paramio, T. Torres, D. K. P. Ng and G. de la Torre, *J. Med. Chem.*, 2023, **66**, 3448–3459.
61 K. Suzuki, Y. Miura, Y. Mochida, T. Miyazaki, K. Toh, Y. Anraku, V. Melo, X. Liu, T. Ishii, O. Nagano, H. Saya, H. Cabral and K. Kataoka, *J. Controlled Release*, 2019, **301**, 28–41.
62 K. Miura, Y. Wen, M. Tsushima and H. Nakamura, *ACS Omega*, 2022, **7**, 34685–34692.
63 V. Ramu, S. Gautam, A. Garai, P. Kondaiah and A. R. Chakravarty, *Inorg. Chem.*, 2018, **57**, 1717–1726.
64 B. Woods, D. Döllerer, B. Aikman, M. N. Wenzel, E. J. Sayers, F. E. Kühn, A. T. Jones and A. Casini, *J. Inorg. Biochem.*, 2019, **199**, 110781.
65 A. Jana, P. Kundu, S. Paul, P. Kondaiah and A. R. Chakravarty, *Inorg. Chem.*, 2022, **61**, 6837–6851.
66 A. Jana, S. Sahoo, S. Paul, S. Sahoo, C. Jayabaskaran and A. R. Chakravarty, *Inorg. Chem.*, 2024, **63**, 6822–6835.
67 X. Zheng, L. Zhang, M. Ju, L. Liu, C. Ma, Y. Huang, B. Wang, W. Ding, X. Luan and B. Shen, *ACS Appl. Mater. Interfaces*, 2022, **14**, 46262–46272.
68 X. Chen, B. B. Mendes, Y. Zhuang, J. Conniot, S. M. Argandona, F. Melle, D. P. Sousa, D. Perl, A. Chivu, H. K. Patra, W. Shepard, J. Conde and D. Fairen-Jimenez, *J. Am. Chem. Soc.*, 2024, **146**, 1644–1656.
69 G. Liang, N. Montesdeoca, D. Tang, B. Wang, H. Xiao, J. Karges and K. Shang, *Biomaterials*, 2024, **309**, 122618.
70 U. Bhattacharyya, B. K. Verma, R. Saha, N. Mukherjee, M. K. Raza, S. Sahoo, P. Kondaiah and A. R. Chakravarty, *ACS Omega*, 2020, **5**, 4282–4292.
71 A. Jana, S. Sahoo, S. Paul, S. Sahoo, C. Jayabaskaran and A. R. Chakravarty, *Polyhedron*, 2023, **245**, 116656.
72 T. Saghatelyan, A. Tananyan, N. Janoyan, A. Tadevosyan, H. Petrosyan, A. Hovhannisyan, L. Hayrapetyan, M. Arustamyan, J. Arnhold, A. R. Rotmann, A. Hovhannisyan and A. Panossian, *Phytomedicine*, 2020, **70**, 153218.

73 K. M. Nelson, J. L. Dahlin, J. Bisson, J. Graham, G. F. Pauli and M. A. Walters, *J. Med. Chem.*, 2017, **60**, 1620–1637.
74 S. Banerjee and A. R. Chakravarty, *Acc. Chem. Res.*, 2015, **48**, 2075–2083.
75 U. Bhattacharyya, B. Kumar, A. Garai, A. Bhattacharyya, A. Kumar, S. Banerjee, P. Kondaiah and A. R. Chakravarty, *Inorg. Chem.*, 2017, **56**, 12457–12468.
76 A. Bhattacharyya, A. Jameei, A. A. Karande and A. R. Chakravarty, *Eur. J. Med. Chem.*, 2021, **220**, 113438.
77 A. Upadhyay, P. Kundu, V. Ramu, P. Kondaiah and A. R. Chakravarty, *Inorg. Chem.*, 2022, **61**, 1335–1348.
78 L. Pan, S. Wang, M. Xie, M. Liang, L. Yu, B. Du, X. Ye, Y. Luo, Y. Y. Quan and Z. S. Huang, *Mater. Des.*, 2023, **235**, 112441.
79 S. Maiti and P. Paira, *Eur. J. Med. Chem.*, 2018, **145**, 206–223.
80 S. Paul, P. Kundu, U. Bhattacharyya, A. Garai, R. C. Maji, P. Kondaiah and A. R. Chakravarty, *Inorg. Chem.*, 2020, **59**, 913–924.
81 S. Paul, P. Kundu, P. Kondaiah and A. R. Chakravarty, *Inorg. Chem.*, 2021, **60**, 16178–16193.
82 A. Bera, A. Nepalia, A. Upadhyay, D. K. Saini and A. R. Chakravarty, *Dalton Trans.*, 2023, **52**, 13339–13350.
83 A. Bera, A. Nepalia, A. Upadhyay, D. K. Saini and A. R. Chakravarty, *Inorg. Chem.*, 2024, **63**, 17249–17262.
84 S. J. He, Y. W. Xie and Q. Y. Chen, *Spectrochim. Acta, Part A*, 2018, **195**, 210–214.
85 S. Xiong, W. Sun, R. Chen, Z. Yuan and X. Cheng, *Carbohydr. Polym.*, 2021, **273**, 118590.
86 A. Hafuka, H. Satoh, K. Yamada, M. Takahashi and S. Okabe, *Materials*, 2018, **11**, 3–11.
87 A. Mondal, S. Mondal, A. Majee and S. Dutta, *New J. Chem.*, 2025, **49**, 9166–9176.
88 H. Wen, Q. Wu, L. Liu, Y. Li, T. Sun and Z. Xie, *Biomater. Sci.*, 2023, **11**, 2870–2876.
89 C. Mou, X. Wang, Y. Liu, Z. Xie and M. Zheng, *J. Mater. Chem. B*, 2022, **10**, 8094–8099.
90 Q. Shi, C. Mou, Z. Xie and M. Zheng, *Photodiagn. Photodyn. Ther.*, 2022, **39**, 102901.
91 P. Dharmaratne, R. C. H. Wong, J. Wang, P. C. Lo, B. Wang, B. C. L. Chan, K. M. Lau, C. B. S. Lau, K. P. Fung, M. Ip and D. K. P. Ng, *Biomedicines*, 2020, **8**, 140.
92 H. Wen, Q. Wu, C. Li, T. Sun and Z. Xie, *ACS Appl. Nano Mater.*, 2022, **5**, 1500–1507.
93 W. J. Peveler, S. Noimark, H. Al-Azawi, G. B. Hwang, C. R. Crick, E. Allan, J. B. Edel, A. P. Ivanov, A. J. MacRobert and I. P. Parkin, *ACS Appl. Mater. Interfaces*, 2018, **10**, 98–104.

